IEEE Access
Multidisciplinary | Rapid Review | Open Access Journal

Received 27 September 2023, accepted 22 October 2023, date of publication 25 October 2023, date of current version 2 November 2023.

Digital Object Identifier 10.1109/ACCESS.2023.3327343

RESEARCH ARTICLE

A Hybrid Local Replanning Strategy for Multi-Satellite Imaging Mission Planning in Uncertain Environments

XUEYING YANG, MIN HU, GANG HUANG, AND ANDI LI
Department of Aerospace Science and Technology, Space Engineering University, Beijing 101416, China

Corresponding author: Min Hu (jlhm09@126.com)

This work was supported by the National Natural Science Foundation of China under Grant 61403416.

ABSTRACT Multi-satellite imaging mission planning (MSIMP) research has advanced substantially in recent years. However, contemporary MSIMP research in uncertain environments is still confronting challenges such as loss of satellite resource allocation, inadequate anti-jamming ability of the mission planning scheme, and low mission completion rate. Therefore, in this work, we propose a hybrid local replanning strategy improved adaptive differential evolutionary (HLRS-MSFADE) algorithm based on the multi-satellite imaging mission planning in uncertain environments (MSIMPUE). First, an MSIMPUE model based on uncertainty assessment is constructed. This model solves the problem of assessing new tasks with varied qualities to decide the observation order in an uncertain environment and decreases the loss caused by inefficient satellite resource allocation. Second, to address the issue of difficulty in planning for changing new task requirements in uncertain environments, an HLRS for uncertain environments is developed to ensure efficient task insertion while avoiding conflict costs. Finally, an MSFADE algorithm is presented to handle the problem of long MSIMPUE mission response time and low mission completion rate with good quality in an acceptable computation time. The simulation results validated the effectiveness and stability of the method in dealing with MSIMPUE. Moreover, the HLRS-MSFADE algorithm outperforms previous methods in terms of mission response time, mission completion rate, and motion perturbation.

INDEX TERMS Uncertain environment, multi-satellite imaging mission planning, replanning strategy, adaptive differential evolutionary algorithm.

I. INTRODUCTION

Multi-satellite imaging mission planning (MSIMP) refers to the optimal allocation of limited satellite resources based on a complex mission environment and varied user requirements to optimize Earth observation operation efficiency and gather remote sensing images [1], [2]. Multiple imaging satellites can achieve long-term and multi-directional continuous monitoring of the observation area through mutual cooperation, and they play an important role in geographical mapping, land resource survey, disaster monitoring, and other fields [3], [4]. However, during the implementation of satellite missions, the environment dynamically changes, influencing a large range of uncertain factors, such as 1) interference of non-partner spacecraft, change of imaging satellite observation demand, and emergency adjustment of satellite resources leading to satellite resource conflict. 2) In the space environment, the orbiting satellite is influenced by solar storms and space debris impact, among others, resulting in satellite attitude loss caused by radiation from electronic components, leading to partial failure of the original plan [5], [6]. As a result, research on Multi-satellite Imaging Mission Planning in uncertain environments (MSIMPUE) has received increased interest. In particular, comprehensive consideration of imaging requirements, such as task requirements, guarantee types, and application fields is urgent to cope with emergencies in uncertain environments and solve the MSIMPUE problem [7], [8].

The associate editor coordinating the review of this manuscript and approving it for publication was Haibin Sun.

In recent years, the integer programming model [9], constraint fulfillment model [10], deterministic algorithm [11], intelligent optimization algorithm [12], and heuristic algorithm [13], [14] have been used in MSIMPUE research. MSIMPUE approaches are currently classified into three types: proactive planning, reactive planning, and proactive reactive planning.

MSIMPUE based on proactive planning. Proactive planning (PP) is an offline mission planning method that develops MSIMP schemes based on prior knowledge in uncertain environments [15]. Li et al. [16] proposed a multi-objective evolutionary algorithm based on the PP of Earth observation satellites to generate a multi-satellite mission planning scheme with certain anti-interference capability. Chen et al. [17] developed a PP strategy based on priority and conflict avoidance to maximize overall mission planning within an acceptable computing time under the competition of diverse satellite resources. Ayana et al. [18] suggested a PP solution that improves the mixed integer linear programming strategy while considerably reducing computational complexity.

MSIMPUE based on reactive planning. Reactive planning (RP) is a type of mission planning that occurs in real-time. During the implementation of the first plan, local replanning of the initial plan is triggered based on uncertain occurrences to build a multi-satellite mission planning scheme [15]. Cui et al. [19] introduced a multi-satellite dynamic RP model based on task priority and solved it using a hybrid genetic tabu search method, which increases the value of observation tasks. Yang et al. [20] proposed a multi-autonomous satellite system with onboard scheduling capabilities in an uncertain environment, which can effectively reduce revenue loss and the number of mission failures. Liang et al. [21] developed a mathematical model based on predicate logic to investigate reactive scheduling space-borne mission planning methods with high scalability.

MSIMPUE based on proactive reactive planning. Proactive Reactive Planning (PRP) is a method of mission planning that consider offline and real-time planning. On the basis of existing knowledge, PRP develops an initial scheme, repairs and adjusts the initial scheme in response to real-time changes, and generates a multi-satellite mission planning scheme [22]. Han et al. [23] proposed a multi-satellite mission planning based on proactive scheduling under an uncertain cloud cover environment to maximize the overall observation benefits. He et al. [24] developed a dynamic distributed organization structure for PRP in dynamic contexts to increase the algorithm's solving efficiency. Lu et al. [25] devised a proactive scheduling multi-satellite mission planning strategy based on regional goals to achieve multi-satellite execution sequences in regions of various sizes.

Although previous studies have produced good planning results, the following issues remain for MSIMPUE:

- An uncertain environment is frequently confronted with various issues, such as a lack of satellite resources and imaging task conflict, due to the batch delivery of new tasks. Based on existing knowledge, determining the sequence for obtaining satellite resources for target tasks involves a high degree of subjectivity, resulting in satellite resource loss. As a result, MSIMPUE faces a problem in properly considering the usage of satellite resources in uncertain environments and developing a mission planning model that reasonably defines the priority of target missions.
- Uncertain environments are influenced by various factors, including mission cancellation, mission attribute changes, and changes in allocated satellite resources, and the number of satellite observation missions, arrival time, and mission type are all uncertain, increasing the difficulty of solving MSIMPUE problems. As a result, MSIMPUE is facing a new challenge: how to create an efficient MSIMP approach for new missions dynamically submitted in unknown circumstances.
- In the MSIMPUE-solving process, many conflicting objectives, such as mission benefit and reaction time must be addressed, which increases issue-solving complexity exponentially, resulting in a long MSIMPUE mission response time and poor mission completion rate. As a result, another issue for MSIMPUE is to fairly trade off the space's search and exploitation performance and build an algorithm to swiftly solve the superior mission planning scheme.

To solve these difficulties, this paper takes imaging satellites as the research object and proposes a hybrid local replanning strategy and multi-strategy fusion adaptive differential evolution algorithm (HLRS- MSFADE) for MSIMPUE. The main contributions of this paper are as follows.

- Aiming at the existence of factors such as changes in imaging requirements and assignment conflicts that affect the planning of multi-satellite imaging missions in uncertain environments, an MSIMPUE model based on uncertainty assessment is proposed. This model converts new missions arriving in batches into a series of new mission sets carrying priority information, reduces losses due to the irrational allocation of satellite resources, and provides a rational allocation of satellite resources.
- Aiming at changing mission requirements in an uncertain environment, a hybrid local replanning strategy (HLRS) for an uncertain environment is proposed. The MSIMPUE problem is transformed into a new mission insertion problem that avoids the cost of conflict as much as possible by adjusting the time window between the new mission and the original satellite observation sequence. It also minimizes the influence of the new task insertion on the original satellite observation sequence to the greatest extent.
- To address the issues of long mission response time and low mission completion rate caused by a large MSIMPUE solution space and numerous constraints, a multi-strategy fusion adaptive differential evolution

(MSFADE) algorithm is proposed. This algorithm aims to solve high-quality MSIMPUE planning schemes within a reasonable calculation time by integrating the mutation strategy and the dynamic mutation rate. It also aims to achieve an effective balance between improved mission planning schemes, fast response times, and reduced perturbations.

The remainder of the paper is structured as follows. Section II discusses the uncertainties that affect MSIMPUE and the basic execution process of MSIMPUE. Section III builds the MSIMPUE model based on uncertainty assessment, which includes the mathematical description, objective function, and model restrictions. Section IV details the HLRS-MSFADE method. Section V examines the effectiveness and stability of the HLRS-MSFADE algorithm for solving MSIMPUE and assesses its performance by comparing tests with several mutation strategies and algorithms. Section VI concludes with a brief overview and recommendations for future research.

II. RELATED WORD

This section initially analyzes the uncertainties affecting MSIMPUE and then introduces the basic execution flow of MSIMPUE.

A. MSIMPUE UNCERTAINTY FACTOR ANALYSIS

Currently, imaging satellites are frequently disturbed by a number of uncertain factors during mission execution [26], [27]. For example, 1) the number of in-orbit satellites in space has increased significantly, which has led to an increase in the satellite collision rate; 2) satellites serving in orbit in the space environment are subject to interference from solar activity and electromagnetic storms, and the satellite failure rate has gradually increased; and 3) the demand for in-orbit satellite reconnaissance missions has grown increasingly complex, and the satellite's mission requirements are susceptible to change. To further clarify the uncertainties that a satellite may be subjected to in the process of performing a mission in an uncertain environment, and to better guide the Multi-Satellite Imaging Mission Planning System in determining the order in which satellites should perform the target mission, this paper categorizes the uncertainties affecting the MSIMPUE into the categories of internal uncertainty and external uncertainty. In Figure 1(a), the black circle represents the target observation task. The satellite observation in different colors indicates that the satellite cannot continuously perform the observation task due to the interference of internal uncertainties, such as satellite load failure, satellite power supply failure, and internal circuit anomaly during task execution, and the original observation task is cancelled. As shown in Figure 1(b), the red dashed line represents the replacement task; the red circle represents task cancellation; and the blue, gray, and purple areas indicate that the original observation task loses its effectiveness when several imaging satellites encounter external uncertainties of cloud cover, user demand change, and mission cancellation during the implementation of the mission planning scheme, respectively. Mission planning plans must be revised to account for changing circumstances. Unidentified factors must be assessed, and realistic mission planning must be performed in response to changing environmental conditions and mission observation requirements. Therefore, the influence of uncertain factors on satellite mission planning must be analyzed, and an effective multi-satellite imaging mission planning method should be designed to cope with uncertain environments.

B. BASIC EXECUTION PROCESS OF MSIMPUE

Assuming that a group of satellites $S = \{S_j | j \in N, N = \{1, \ldots, n\}\}$ perform a group of observation tasks $T = \{t_i | i \in N_T, N_T = \{1, \ldots, m\}\}$, the optimal satellite observation sequence to generate the initial mission planning is $\{m_1, m_2, m_3, m_4\}$. The initial mission planning is shown in Figure 2(a), multiple satellites S_j operate in orbit $Oribt_o$, and the satellites perform assigned target tasks t_i in orbits

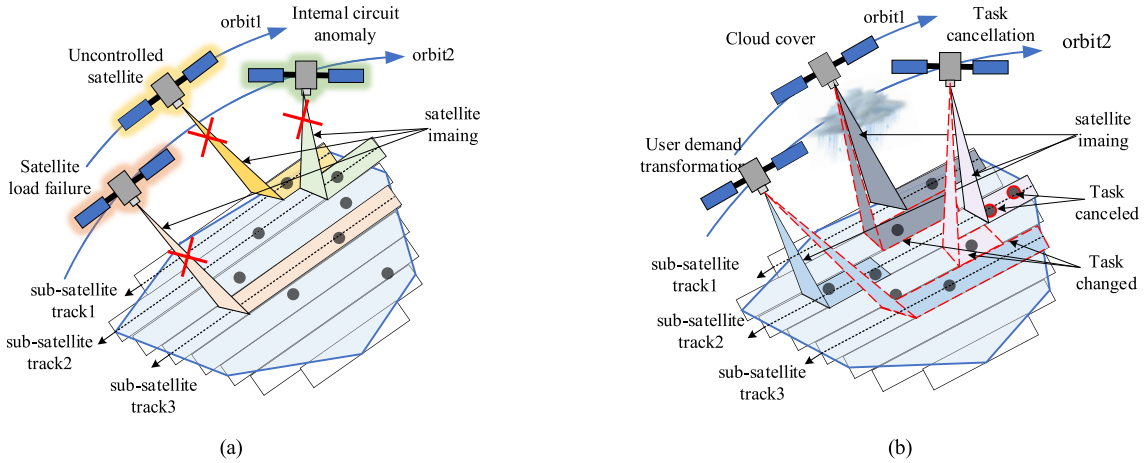

FIGURE 1. Satellite in an uncertain environment. (a) Internal environment uncertainty situation; (b) External environment uncertainty situation.

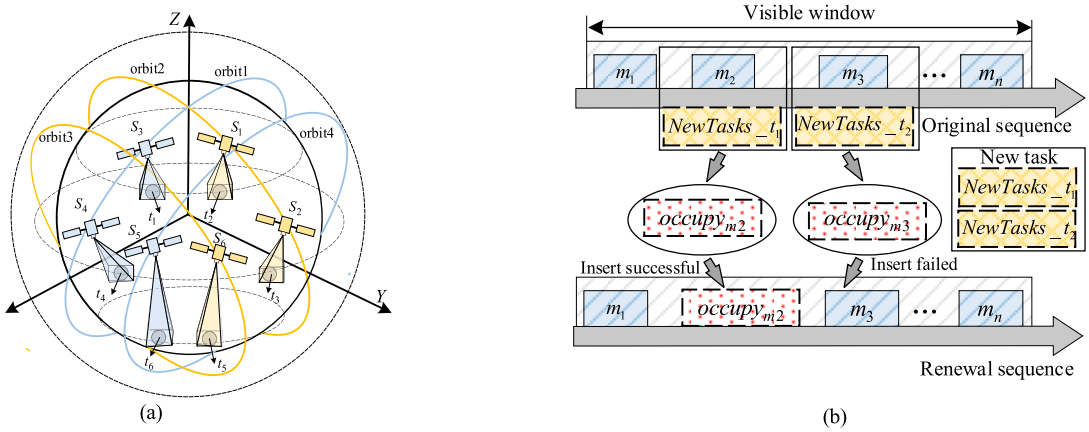

FIGURE 2. Illustration of multi-satellite mission planning. (a) initial mission planning process; (b) New task add to MSIMPUE.

within the time window. In an uncertain environment, when a batch of new tasks $NewTasks = \{NewTasks\_t_1, NewTasks\_t_2\}$ arrives at time T, the new tasks must be synthesized into the original satellite observation sequence on the basis of the initial mission planning scheme to produce an executable new mission planning scheme. As shown in Figure 2(b), the new task $NewTask\_t_i$ and task m_i are synthesized. If the multi-satellite imaging constraints are met, then the new task will be successfully inserted into the original satellite observation sequence as a composite task; otherwise, the original task will be maintained, and the MSIMPUE scheme will be generated by repeating this step. The new satellite observation sequence is $\{m_1, occupy_{m2}, m_3, m_4\}$ [28], [29].

III. PROBLEM DESCRIPTION

This section initially introduces the MSIMPUE model based on uncertainty assessment and then further describes the objective function of the MSIMPUE model and its constraints.

A. MSIMPUE MODEL BASED ON UNCERTAINTY ASSESSMENT

The MSIMPUE problem can be described as follows. According to the information of the satellite resource set $Sat = \{s_1, s_2, s_3, \ldots, s_n\}$ and task set $Initial_{Tasks} = \{t_1, t_2, t_3, \ldots, t_N\}$ in the initial environment, the uncertainty factors of the initial task are evaluated and analyzed to determine its priority $Ptarget$. On the basis of the objective function and target constraints, the tasks $\{m_1, m_2, m_3, \ldots, m_g\}$ on the j orbit o of the satellite that meet the synthesis constraints are combined, and the composite task is expressed as $occupy = \{j, o, st, et, \theta_a, [m_1, m_2, m_3, \ldots, m_g]\}$. An improved adaptive differential evolution (DE) algorithm is used to generate an initial multi-satellite mission planning scheme $schedule = \{occupy_1, \ldots, occupy_n\}$. Particularly, the specific methods of the MSIMPUE model based on uncertainty assessment are as follows.

A unified mathematical description of the uncertainty evaluation index is expressed as follows:

$$w = f(\prod_{i=1}^{n} X_i) = f(T_U, I_U, D_U, R_U, N_U), \tag{1}$$

where w is the task weight coefficient, T_U is the type of the uncertainty factor, I_U is the intensity of the uncertainty factor, D_U is the urgency of the uncertainty factor, R_U is the benefit of the new task, and N_U is the number of the uncertainty factors contained in a single new task.

The judgment matrix of the evaluation model for uncertainty factors is expressed as:

$$B = \begin{bmatrix} 1/B_{11} & 1/B_{12} & \ldots & 1/B_{1n} \\ 1/B_{21} & 1/B_{22} & \vdots & 1/B_{2n} \\ \vdots & \vdots & & \vdots \\ 1/B_{n1} & 1/B_{n2} & \cdots & 1/B_{nn} \end{bmatrix} \tag{2}$$

where B_{ij} is the relative importance between indicators i and j, as follows:

$$B_{ij} = \begin{cases} 0, & factor\ i \text{ is less important than } j \\ 0.5, & \text{as significant as } factor\ i \text{ and } j \\ 1, & factori \text{ is important than } factor\ j \end{cases} \tag{3}$$

The calculation function of the task weight coefficient of the uncertainty factor evaluation is as follows:

$$w(X_1, X_2, X_3, X_4, X_5) = \sum_{i=1}^{n} \sum_{j=1}^{n} B_{ij} X_i \tag{4}$$

where X_i represents the i-th evaluation index of the uncertainty factors, as shown as follows:

$$\text{Priority} = 10 \cdot \frac{w(X_i) \cdot B_{ij} \cdot (1 - \prod_{j=1}^{n} (1 - B_{ij})}{\sum_{i=1}^{n} \sum_{j=1}^{n} B_{ij}} \tag{5}$$

TABLE 1. Evaluation index of uncertain factors affecting MSIMP in uncertain environments.

ID	Evaluation indicator	Mathematical description	Explanation
X_1	Type of uncertainty factor	$T_U = \begin{Bmatrix} Attitude_u, Payload_u, Cloud_c, \\ \mathrm{Re}solution_C, Demand_C, mission_c \end{Bmatrix}$	Uncertainty factors include satellite attitude loss $Attitude_u$, satellite load failure $Attitude_u$, cloud cover. $Cloud_c$., mission resolution change $\mathrm{Re}solution_C$, user mission replacement $Demand_C$, and mission cancellation $mission_c$.
X_2	Intensity of uncertainty	$I_U = \{I_S, I_M, I_L\}$	The occurrence intensity of uncertainty factors can be categorized into strong I_S, medium I_M, and weak I_L.
X_3	Degree of mission urgency	$D_U = \{D_S, D_R, D_c\}$	The urgency of the uncertain event can be categorized into serious D_S, heavy D_R, and routine D_c.
X_4	Task revenue	$R_U = \{R_H, R_M, R_L\}$	The new task benefit can be categorized into high benefit R_H, medium benefit R_M, and low benefit R_L.
X_5	Uncertain numbers in a single task	$N_U = \{N_M, N_c, N_S\}$	The number of uncertain factors contained in a single uncertain event can be categorized into more N_M, general N_c, and less N_S.

which defines the priority of the target task according to the evaluation results of uncertain factors. The evaluation indicators of the MSIMPUE uncertainties used in this study are listed in Table 1.

The satellites are then executed according to the initial multi-satellite mission planning system. If various new tasks arrive in batch processing at time T, through the MSIMPUE model based on the assessment of uncertainties, satellite controllers can update the indicators of uncertainties based on the needs of actual changes in the situation. As shown in Table 1, Specifically contains the type of uncertainty factor T_U, intensity of uncertainty I_U, degree of mission urgency D_U, task revenue R_U, and uncertain numbers in a single task N_U. Generate priorities for satellite execution target missions that can be dynamically updated based on uncertain environmental changes and the new tasks are converted into a series of new task sets $NewTasks = \{t_1, t_2, t_3, \ldots, t_{N_{ntask}}\}$ carrying priority information. The initial mission planning scheme is partially replanned using the HLRS. The MSIMPUE scheme is obtained for new task insertion $newschedule = \{noccupy_1, \ldots, noccupy_n\}$.

B. ESTABLISHING MSIMPUE OBJECTIVE FUNCTIONS AND CONSTRAINTS

1) OBJECTIVE FUNCTIONS

This work focuses on three components of objective function construction: mission benefit, response time, and perturbation cost. Mission benefit denotes the total priority of the satellite to execute the target task in an uncertain environment, response time denotes the total response time of each satellite to complete the target task, and perturbation cost denotes the effect of new task insertion on the initial mission plan throughout the entire MSIMPUE process. The MSIMPUE's objective function is constructed as follows.

- Mission benefit objective function

$$\max f_1(x_{ijk}, nx_{ijk}) = \sum_{i=1}^{N_{task}} \sum_{j=1}^{N_S} (\sum_{k=1}^{N_o} x_{ijk} \cdot priority_{task} + \ldots + \sum_{i=1}^{N_{ntask}} nx_{ijk} \cdot priority_{ntask}), \quad (6)$$

where x_{ijk} represents the decision variable of each satellite and the initial target mission, nx_{ijk} represents the decision variable of each satellite and the new target mission, $priority_{task}$ represents the priority of the initial target task $task_i$, $priority_{ntask}$ represents the priority of the new task $ntask_i$, N_{task} represents the number of the initial target mission, N_{ntask} represents the number of the new target tasks, N_S represents the number of satellites to be executed, and N_o represents the number of orbits.

- Response time objective function

$$\min f_2(x_{ijk}, nx_{ijk}) = \frac{\sum_{i=1}^{N_{task}} \sum_{j=1}^{N_S} (\sum_{k=1}^{N_o} x_{ijk} \cdot Time_{res}^i + \sum_{k=1}^{N_o} nx_{ijk} \cdot nTime_{res}^i)}{N_{task} + N_{task}} \quad (7)$$

where $Time_{res}^i$ represents the response time of the initial target task, and $nTime_{res}^i$ represents the response time of the new task.

- Perturbation cost objective function

$$\min f_3(perx_{i,\alpha}) = \sum_{i=1}^{N_{ntask}} perx_{i,\alpha} \cdot \alpha, \quad (8)$$

where $perx_{i,\alpha}$ represents the disturbance decision variable, and α represents the disturbance degree. The disturbance level is mainly considered in four cases, namely, unchanged number of synthetic tasks, increased number of synthetic tasks, and replacement or deletion of synthetic tasks compared with the original satellite observation sequence, which

can be described as follows:

$$\alpha = \left\{ \begin{array}{l} \omega_1, w_{ijk}^t \text{remain the same, } con\_t/\theta_a \text{ change} \\ \omega_2, w_{ijk}^t \text{incresed numbers} \\ \omega_3, w_{ijk}^t \text{haved changed} \\ \omega_4, \text{Task replacement/Delete} \end{array} \right\} \quad (9)$$

where w_{ijk}^t is the time window corresponding to the execution of target mission i by satellite S_j in orbit $Orbit_o$. The disturbance degree range is $0 \leq \omega_1 \leq \omega_2 \leq \omega_3 \leq \omega_4 \leq 1$.

The global optimization objective function is generated using the above objective function and the constraint violation cost, as shown as follows:

$$\max f = \mu \cdot f_1 - \lambda f_2 - \tau f_3 - \beta \sum_{i=1}^{I} c_i \quad (10)$$

where μ, λ, τ, and β are the scale scaling factors of mission benefit, response time, perturbation cost, and constraint violation cost, respectively, and all remain of the same order. c_{i} is the penalty function corresponding to the violation of the constraint, and I is the constraint condition. Solving the optimal mission planning scheme for MSIMPUE is a class of multi-objective decision problems, in which the constructed global optimal objective function is dynamically adapted to different multi-satellite imaging mission planning scenarios by setting the weights of μ, λ, τ, and β to be adjusted according to the actual environment and the user's demand preference.

2) CONSTRAINT FUNCTIONS

This section defines and explains the MSIMPUE model's constraints.

- Uniqueness constraints

$$\sum_{i=1}^{N_{task}} \sum_{j=1}^{N_S} \sum_{k=1}^{N_O} t_{ijk} \leq 1, \forall t_i \in \text{Initial}Tasks \cup NewTasks \quad (11)$$

Task t_i has a visible time window on multiple satellite resources, but it can only be executed by one of them.

- Frequency of satellite side swing imaging in a single orbit constraint

$$\forall orbit_i \in Orbit, Orbit = \{orbit_1, \ldots, orbit_o\}, N_i \leq N_{Oi} \quad (12)$$

The number of satellite yaw imaging in any orbit cycle N_i is less than the maximum number of satellite yaw imaging in a single orbit cycle N_{Oi}.

- Maximum side swing angle constraint

$$|\theta_a| \leq A_j, \theta_a \in occupy \cup tempoccupy \quad (13)$$

The absolute magnitude of the yaw angle of any synthetic mission θ_a must not exceed the maximum yaw angle of the satellite A_j due to limited satellite resources.

- Time constraint of satellite attitude conversion

$$\left| \theta_a^{j,o,k+1} - \theta_a^{j,o,k} \right| / \omega_j < st_{k+1}^{j,o} - st_k^{j,o},$$
$$j \in S, o \in O, k \in \text{Initial}Tasks \cup NewTasks \quad (14)$$

The attitude conversion between two adjacent synthesis activities in the same orbit must occur within the conversion time.

- Imaging duration constraints

$$et_k^{j,o} - st_k^{j,o} \leq d_j, j \in S, o \in O,$$
$$k \in \text{Initial}Tasks \cup NewTasks \quad (15)$$

Any synthetic task until the end time $et_k^{j,o}$ and start time $st_k^{j,o}$ should be less than or equal to the difference between the satellite remote sensor's longest single boot time d_j.

- Resolution constraints

$$\forall w_{ijk}^t \cup nw_{ijk}^t, r_j^S \leq r_{\min} \quad (16)$$

Any time window of satellite observation $\forall w_{ijk}^t \cup nw_{ijk}^t$ needs to meet the resolution r_j^S of satellite remote sensor, which is less than or equal to the minimum resolution $r_{\min}$ required by satellite imaging users.

- Field angle constraints

$$\forall m_i \in (occupy_k^{jo} \cup noccupy_k^{jo}), |m_i\_\theta_a - m_{i-1}\_\theta_a| \leq \theta_j \quad (17)$$

Any single task m_i must be within the single field angle θ_j of the satellite remote sensor at the same time due to limited satellite resources.

IV. DESIGN OF HLRS-MSFADE ALGORITHM

This section proposes a hybrid local replanning strategy improved adaptive differential evolutionary (HLRS-MSFADE) algorithm based on MSIMPUE. The HLRS-MSFADE is divided into two pieces using the layer-by-layer breakdown concept. The first part evaluates and analyzes the uncertainty aspects of the initial mission to establish its priority, and an MSFADE algorithm is utilized to solve the initial multi-satellite mission planning scheme of the MSIMPUE output. In the second part, an HLRS inserts a new task containing priority information into the initial multi-satellite mission planning scheme. The optimal MSIMPUE solution is generated using an MSFADE algorithm. Algorithm 1 depicts the HLRS-MSFADE algorithm framework.

A. HYBRID LOCAL REPLANNING STRATEGY

To meet the changing mission requirements in an uncertain environment, it is difficult to adapt the global replanning approach to MSIMPUE, resulting in the failure of multi-satellite observation missions. To reduce the disruption to mission planning, an HLRS for uncertain environments is developed, which modifies the initial mission planning scheme while retaining the original satellite observation sequence. It consists of four sequential task insertion methods: synthetic insertion with no conflicting costs method

Algorithm 1 Framework of HLRS-MSFADE

Input: *obj* (Parameters of the satellites S_n, Parameters of the new tasks N_n, Parameters of the basic tasks$occupy_n$, Population size P_n, Random sequence population Rs

Output: MSIMPUE optimal scheme under an uncertain environment

1 Construct the MSIMPUE model based on uncertainty assessment to generate a new task set
$NewTasks = \{t_1, \ldots, t_{N_{ntask}}\}$;
2 Build the MSIMPUE fitness function using Equations (6)–(10) and the constraints using Equations (11)–(17);

$$3\ \max f = \mu \cdot f_1 - \lambda f_2 - \tau f_3 - \beta \sum_{i=1}^{I} c_i;$$

4 /* Use the HLRS-MSFADE to obtain the MSIMPUE optimal initial scheme under the uncertain environment */
$Solu = HLRS - MSFADE\_operate(occupy, Rs)$;
for *gen=1:n*
$Mu = MutationOperator(Rs)$; /* *Mutation Operator*/
$Cr = CrossoverOperator(Mu)$; /* *Crossover Operator*/
$MSFADE\_f = SelectionOperator(Cr)$/*Selection Operator*/
end
$schedule = \{occupy_1, \ldots, occupy_n\}$ % initial scheme
5 /* Hybrid local replanning strategy */
if $NewTasks \neq \emptyset$
$newpop = HLRS\ \{NewTask(i:), schedule(j:)\}$;
$newSchedule = Phase1\_MutationOperator(newpop)$;
else output MSIMPUE optimal scheme;
end
7 ***end***

(SINCCM), independent insertion with no conflicting costs method (IINCCM), iterative insertion to avoid conflicting costs method (IIACCM), and alternative insertion to minimize conflict costs method (AIMCCM).

1) INSERT METHOD 1: SINCCM

SINCCM is the simplest in the HLRS. It inserts new tasks into the original satellite observation sequence as meta-tasks of synthetic tasks. It can be used to avoid the conflict cost between the HLRS and the original satellite observation sequence meta-task without changing the task execution time window. Assume that the observable time window of the new task $\{t_1, t_2, t_3\}$ in the new task set $NewTasks = \{t_1, t_2, t_3, \ldots, t_{N_{ntask}}\}$ is in satellite S_{j1} in orbit O_{o1}, and the scheduled observation task of the original observation sequence of the satellite on satellite S_j in orbitO_o is $\left\{occupy_{k-1}^{j1,o1}, occupy_k^{j1,o1}, occupy_{k+1}^{j1,o1}\right\}$. A quintuple $pos = [j, o, 1, k, n]$ is used to mark the insertion location with specific information (satellite number, orbit number, presence of a composite task, insertion location number, and task number).

Figure 3 shows the schematic of the SINCCM in the HLRS for uncertain environments. First, the viewable time windows of the original satellite observation sequence in satellite S_{j1} in orbit O_{o1} are visited. The starting position of the new task and each meta-task is then appraised one by one according to the priority of the new work, and the location satisfying the MSIMPUE constraint is placed as the composite insertion point. It contains three type of insert position: Synthetic insertion position 1, in which the new task is inserted before the first meta-task of the synthetic task $occupy_{k-1}^{j1,o1}$; Synthetic insertion position 2, in which the new task is inserted into a meta-task between m_3 and m_4 for the synthesis of task $occupy_k^{j1,o1}$; and Synthetic insertion position 3, in which the new task is inserted after the synthesis task of meta-task m_5 after task $occupy_{k+1}^{j1,o1}$. Finally, a new satellite observation sequence is formed by inserting a new task into the original satellite observation sequence.

2) INSERT METHOD 2: IINCCM

The IINCCM in the HLRS is relatively easy. This method inserts the new task as a separate synthesis task into the original satellite observation sequence and is appropriate when the application of the aforementioned SINCCM conflicts with the original satellite observation sequence and the meta-task. Assuming that the visible time window of the new task set $\{t_4, t_5, t_6\}$ is in satellite S_{j2} in orbit O_{o2}, the insertion of SINCCM has a conflict cost $con1$ with the synthesis task $\left\{occupy_{k-1}^{j2,o2}, occupy_k^{j2,o2}, occupy_{k+1}^{j2,o2}\right\}$ in the original satellite observation sequence. Figure 4 shows the IINCCM in the HLRS for uncertain environments.

First, all the synthesis tasks in satellite S_{j2} in orbit O_{o2} are traversed to obtain the original observation sequence. Then, the starting position of the new task and each synthesis task $occupy^{j2,o2}$ is determined in turn, and the position satisfying the MSIMPUE constraint after insertion is defined as the independent insertion position. It includes: Independent insertion position 1, in which the first task is inserted before the observation sequence synthesis mission of the original satellite $occupy_{k-1}^{j2,o2}$; Independent insertion position 2, in which the new task is inserted between two adjacent synthetic tasks $occupy_{k-1}^{j2,o2}$ and $occupy_k^{j2,o2}$; and Independent insertion position 3, in which the new task is inserted after the last synthetic task of the observation sequence of the original satellite $occupy_{k+1}^{j2,o2}$. Finally, the new task is inserted into the original observation sequence as an independent composite task to generate a new satellite observation sequence.

3) INSERT METHOD 3: IIACCM

The IIACCM is complex in the way new tasks are inserted in the HLRS. This method iteratively inserts new tasks by constructing a virtual task pool that is applicable to cases in which the new task adopts SINCCM and IINCCM. SINCCM and IINCCM have conflicting costs with the original satellite observation sequences, and the conflicting costs generated by the insertion of new tasks are eliminated as far as possible. New tasks are iterated in the simulated task pool, conflicting tasks are stored in the virtual task queue in order of priority, and the task t_8 is one of the conflicting tasks $t_8 \in S_{i\_conflict}$. Figure 5 shows the IIACCM in the HLRS for uncertain environments.

First, the new task t_8 is traversed to obtain imaging resource information for all visible time window. Second, the conflict relationship between the new task t_8 and the original satellite

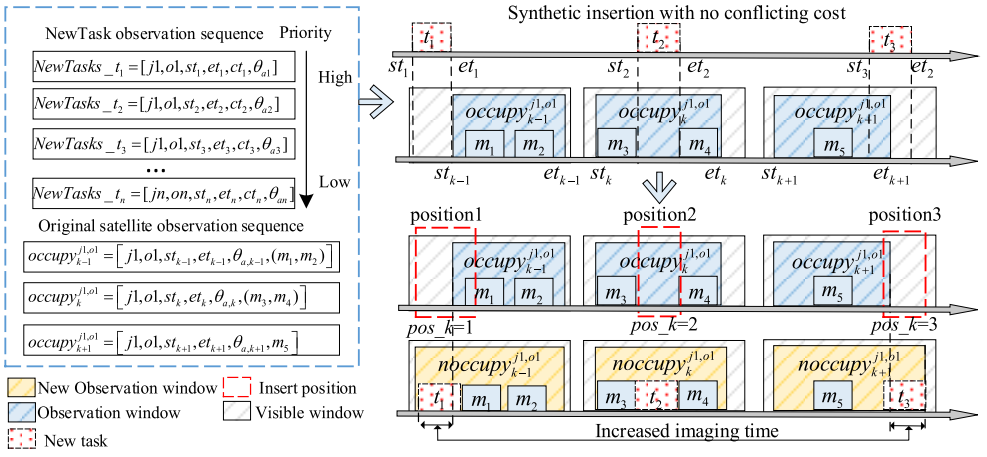

FIGURE 3. Schematic of SINCCM.

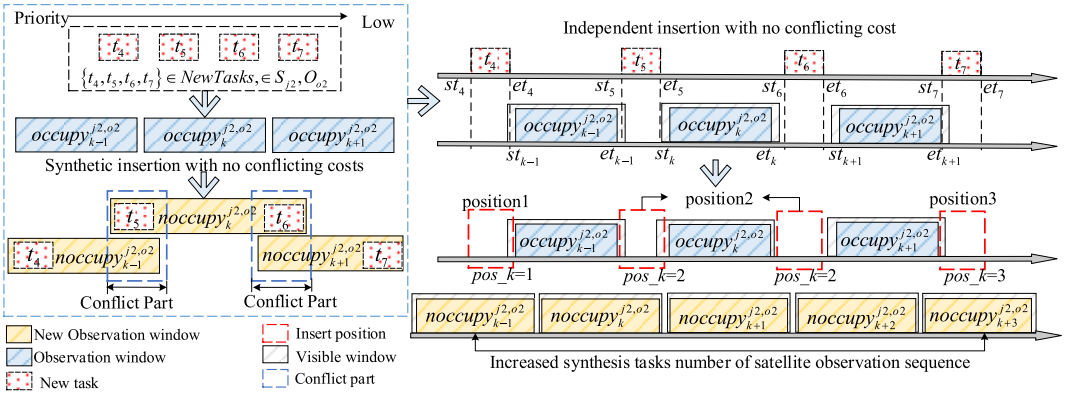

FIGURE 4. Schematic of IINCCM.

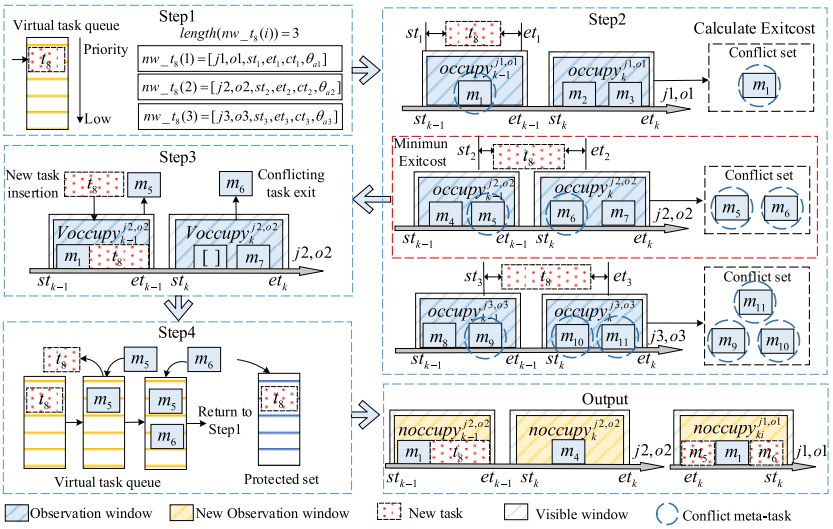

FIGURE 5. Schematic of IIACCM.

observation sequence is examined one by one to calculate the exit cost of the new task's insertion, which results in the withdrawal of the scheduled mission. Third, the time window with the least costly exit is selected to insert the new task t_8, and the exit task is m_5, m_6. Finally, the exit task m_5, m_6 is sequentially inserted into the virtual task queue in order of priority from high to low, and a protection stack is set up to store the newly inserted task to avoid its deletion during

the iteration process. The iteration is then repeated until the virtual task queue is empty, and the output of the new task is inserted into the observation sequence.

The exit cost is defined as the total benefit of existing the tasks, which can be expressed as follows:

$$\text{Exitcost(i)} = \text{e} + \sum_{i=1}^{e} \frac{ptarget_{ci}}{Vtempoccupy\_tw_i} \tag{18}$$

where $S_{i\_conflict} = \{c_1, \ldots, c_e\}$ is the set of conflicting tasks, $ptarget_{ci}$ denotes the priority of the conflicting tasks, and $Vtempoccupy\_tw_i$ is the visible time window of the conflicting tasks. The introduction of an exit cost allows for the exit of scheduled synthetic meta-tasks with smaller task priorities and larger execution time windows. The iterative optimization procedure for minimizing the conflict cost lowers the possibility of exiting the task rescheduling progressively, and the maximum iteration depth is set to 10. As a result, the new high-priority work is always replaced out of the low-priority activity that has a conflict in the original satellite observation sequence during the IIACCM.

4) INSERT METHOD 4: AIMCCM

The AIMCCM is applicable to new task insertion when conflict cannot be avoided by changing the task execution window, that is, the insertion of a new task is bound to create conflict costs. By calculating the conflict cost of the new task in each time window and selecting the time window with the smallest conflict loss for task replacement to minimize the conflict cost, the conflicting task is replaced with the new task if the conflict cost generated by the new task insertion is less than the sum of the gains of the conflicting tasks; otherwise, the new task insertion is cancelled.

Conflict cost is an important impact factor of MSIMPUE. If the insertion of a new mission causes a conflict with the original satellite observation sequence mission and the conflict cannot be avoided by moving the time window, then the insertion of the new mission reduces the total mission benefit of the MSIMPUE scheme. The reduction in the mission benefit is defined as the conflict cost, as shown as follows:

$$\begin{aligned}\text{Conflictcost} = {} & x_{insert}\,\delta\, priority_{ntask} \\ & + (1 - x_{insert}) \sum_{i=1}^{e} priority_{task}\end{aligned} \tag{19}$$

where x_{insert} is the decision factor for new task insertion, $x_{insert} = 0$ indicates the success of new task insertion, $x_{insert} = 1$ denotes the failure of new task insertion, δ is the high-priority task reward factor, $priority_{ntask}$ is the new task priority, and $priority_{task}$ is the task priority. The details of hybrid local replanning strategy are described in Algorithm 2.

B. MULTI-STRATEGY FUSION ADAPTIVE DIFFERENTIAL EVOLUTION ALGORITHM

Differential evolution (DE) is a robust and efficient heuristic evolutionary technique that is highly competitive for solving

Algorithm 2 Hybrid Local Replanning Strategy

Input: Synthesis task of original satellite observation sequences $occupy = \{occupy^{j1,o1}, \ldots, occupy^{jn,on}\}$, Meta-task sequences for synthetic tasks $occupy_k^{ji,oi} = \{occupy_{k,1}^{ji,oi}, \ldots, occupy_{k,g}^{ji,oi}\}$, New task sequences $NewTask = \{t_1, t_2, \ldots, t_{N_{ntask}}\}$

Output: MSIMPUE scheme

/* Synthetic insertion with no conflicting costs */
1 ***for*** $i = 1$: N_{ntask} % Traversing new tasks
2 ***for*** n =1: length $nw\_t(i)$
3 ***for*** k =1: length $occupy_{k,g}^{jo}$
4 Determine the new task's location with $occupy_k^{jo}$.
Insert a new task that meets the MSIMPUE constraints.
$noccupy_k^{jo} = SI_{noconflict}\left\{occupy_k^{jo}(g), t(i)\right\}$;
5 ***else*** $S_{i\_conflict} = \{c_1, \ldots, c_e\}$; % Conflict task sets
6 ***end***
7 ***end***
/* Independent insertion with no conflicting costs */
8 ***if*** $S_{i\_conflict} \neq \emptyset$
9 ***for*** $k = 1$: length $occupy_k^{jo}$
10 Determine the new task's location with $occupy^{j,o}$.
$noccupy_k^{jo} = II_{noconflict}\left\{occupy^{jo}(k), nt(i)\right\}$
11 ***else*** $S_{i\_conflict} = \{c_1, \ldots, c_e\}$;
12 ***end***
13 ***end***
/* Iterative insertion to avoid conflicting costs*/
14 ***if*** $S_{i\_conflict} \neq \emptyset$
15 Building virtual simulation task pools $Vtempoccupy_1$
16 ***for*** k =1: length $S_{i\_conflict}$
17 Exitcost(i)=e+ $\sum_{i=1}^{e} \frac{\text{ptarget}_{ci}}{Vtempoccupy\_tw_i}$
18 $Vtask\_queue\{i, 1\} = sort[occupy_{k,1}^{jo}, \ldots occupy_{k,e}^{jo}]$;
19 repeat Steps 15–18
20 output current virtual scheme
$noccupy_k^{jo} = II_{noconflict}(Vtempoccupy\left\{occupy^{jo}(k), nt(i)\right\})$;
21 ***end***
22 ***end***
/* substitutive insertion with conflicting costs */
23 ***if*** $S_{i\_conflict} \neq \emptyset$
24 ***for*** $n = 1$: length $nw(i)$
25 calculate the conflict cost for new task insertion
Conflictcost $= x_{insert}\,\delta\, priority_{ntask} + (1 - x_{insert}) \sum_{i=1}^{e} priority_{task}$;
26 choose the task with minimum conflict cost
Min(Conflictcost, $\sum_{i=1}^{e} c_i$);
27 $noccupy_k^{jo} = SuI_{conflict}\left\{occupy^{jo}(k), nt(i)\right\}$
28 ***else*** $noccupy_k^{jo} = occupy^{jo}$;
29 ***end***
30 ***end***
31 ***end***

difficult constrained multi-objective optimization problems [9], [30]. Enhanced DEs for MSIMPUE are preference-based, concentrating on either optimization exploration (obtaining more satellite mission planning schemes) or convergence (shorter response time).

Furthermore, determining the *CR* value in DE requires mature a priori knowledge. In addition, the current MSIMPUE using improved DE only investigates the mutation and selection operators, and has not considered the effect of the *CR* value on the mutation strategy. However, the *CR* for MSIMPUE needs to be adjusted according to the algorithm's evolution, and a fixed-value *CR* will result in the algorithm not being able to approach the optimal solution or falling into a local optimum. Therefore, this section proposes a multi-strategy fusion adaptive differential evolutionary algorithm (MSFADE), which adjusts the balance of the algorithmic search by introducing the fusion mutation strategy and dynamic mutation rate to effectively improve the efficiency of the algorithmic search.

First, the mutation strategy used for the fusion mutation strategy is as follows:

- "DE/current-to-rand/1"

$$v_{i,g}(t) = x_{i,g} + F \cdot (x_{r1,g} - x_{i,g}) + F \cdot (x_{r2,g} - x_{r3,g}) \quad (20)$$

- "DE/current-to-pbest/1"

$$v_{i,g}(t) = x_{i,g} + F \cdot (x_{pbest,g} - x_{i,g}) + F \cdot (x_{r1,g} - x_{r2,g}) \quad (21)$$

Figure 6 depicts the schematic of the mutation strategies DE/current-to-pbest/1 and DE/current-to-rand/1 in two dimensions. The Figure 6 indicates that explosiveness and exploration constrain each other in the evolution process due to the varying DE parameters applied to different problems. Excessive exploration leads to the algorithm failing to approach the ideal solution, and excessive explosibility may cause the algorithm to fall into local optimum. Moreover, the mutation approach chosen has a significant effect on algorithm convergence.

Second, to explore and develop the balance algorithm well, the dynamic mutation rate of the algorithm's search balance should be adjusted. The *CR* value is determined as follows:

$$CR(x) = (\log(x)/\log(n))^{\alpha}, x = 1, \ldots, n, \alpha = 1, 2, \ldots, m \quad (22)$$

where x represents the current number of iterations, n epresents the total number of iterations, and α is the curvature change index.

The curve of the dynamic crossover rate changing with different curvature change indices is shown in Figure 7. As shown in Figure 7, an extremely small value causes the dynamic crossover rate to rapidly decline in the early stages of evolution. Then, the proportion of exploration with random search rapidly approaches that of development with fine search, resulting in poor population development and an easy fall into local optimality. An extremely high number causes the dynamic crossover rate to be more exploratory than exploitable early in evolution. Then, the percentage of exploitation with refined search rapidly approaches that of exploration with random search, making convergence problematic.

The crossover operator promotes the exploratory technique for global optimization in the early stages of evolution because the CR value is large. As the number of iterations increases, the CR value approaches zero, and the crossover operator focuses on the exploitative technique for local optimization. Consequently, new individuals are created using the dynamic crossover rate and fusion mutation strategy.

$$v_{i,g}(t) = \begin{cases} \text{DE/current-to-rand/1}, & CR(t) \geq rand[0, 1] \\ \text{DE/current} - \text{to} - \text{pbest/1}, & CR(t) < rand[0, 1] \end{cases} \quad (23)$$

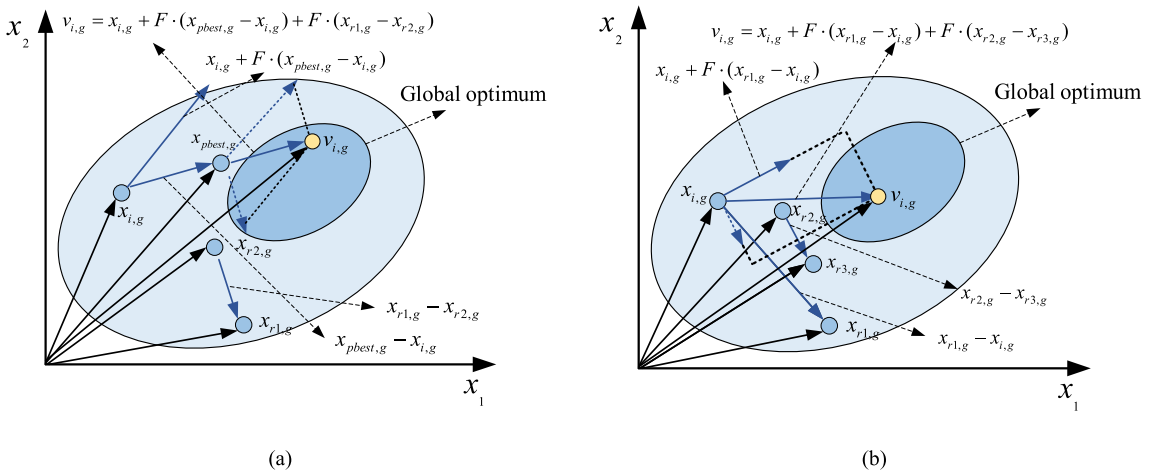

FIGURE 6. Illustration of mutation strategy. (a) DE/current-to-pbest/1; (b) DE/current-to-rand/1.

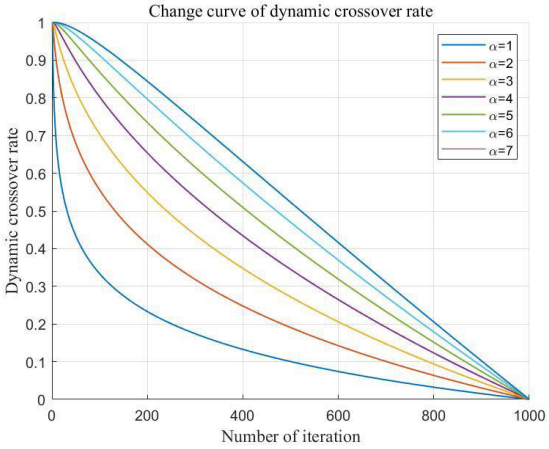

FIGURE 7. Change curve of dynamic crossover rate.

Furthermore, given the size of the scaling factor F value directly influences the algorithm's global optimization capabilities, the dynamic scaling factor is set in the evolution process as follows:

$$F(t) = \begin{cases} 2CR(t), & CR(t) \geq rand[0,1] \\ (2 - CR(t))/2, & CR(t) < rand[0,1] \end{cases} \quad (24)$$

At the early stage of evolution, the mutation strategy DE/current-to-rand/1 with stronger global search capability is chosen to quickly identify the optimal solution region in the space and obtain optimal MSIMPUE solution sets. Then, after the evolution iteration has reached a certain degree, the mutation strategy DE/current-to-pbest/1 with better convergence capability is chosen to ensure that the fine search tends to dominate in the final stage of search. After a specific amount of evolutionary iteration, the mutation strategy DE/current-to-pbest/1 with strong convergence ability is chosen to ensure that the fine search tends to dominate in the last stage of the search, and the optimal MSIMPUE solutions are obtained in a reduced reaction time.

V. COMPUTATIONAL EXPERIMENTS

Four sets of simulation tests are conducted to verify the effectiveness and stability of the HLRS-MSFADE algorithm in MSIMPUE processing. Experiment 1 determines the effectiveness of the MSIMPUE model based on uncertainty assessment, Experiment 2 determines the effectiveness and stability of MSIMPUE with small-scale new task insertions, Experiment 3 establishes the effectiveness and stability of MSIMPUE with large-scale of new task insertions, and Experiment 4 analyzes the performance of the HLRS-MSFADE algorithm.

A. EXPERIMENT SETTINGS

The simulation scenario is constructed to generate eight imaging satellites on May 8, 2023 based on the needs of the multi-satellite imaging mission and the parameters of the launched commercial optical remote sensing satellites. The simulation time is from 00:00:00 to 24:00:00 (UTCG). The satellite orbital and payload parameters are listed in Table 2. Furthermore, the experimental parameters set the population individual size to 50, the maximum number of iterations to 1000 generations.

B. EXPERIMENT 1: EFFECTIVENESS OF THE MSIMPUE MODEL BASED ON UNCERTAINTY ASSESSMENT

To verify the effectiveness of the MSIMPUE model based on uncertainty assessment, 30 imaging target are randomly produced to imitate the tasks required by users. The MSIMPUE model based on uncertainty assessment (MSIMPUE-UA) and the Fixed priority setting method (FPSM) are used to participate in the solution of the MSIMPUE. We refer to the literature [31] for a fixed priority setting approach assuming an uncertain environment with a task priority order of: Major mission requirements ($Priority = 10$) > emergency contingency ($Priority = 9$) > Satellite payload failure ($Priority = 8$) > Satellite power failure ($Priority = 7$) > Internal circuit abnormality ($Priority = 6$) > cloud cover ($Priority = 5$) > User demand change ($Priority = 4$) > Routine mission observations ($Priority = 3$) > scientific experimental observation ($Priority = 2$) > Mission cancelled ($Priority = 1$). Among them, satellite load failure, satellite power supply failure, and internal circuit anomalies necessitate the rapid deployment of satellites to replace problematic satellites for observation, and hence have a high priority.

At the initial moment, the 30 target tasks employ the set of tasks containing target priority information $NewTasks = \{t_1, t_2, t_3, \ldots, t_{N_{ntask}}\}$ generated by MSIMPUE-UA and APSM, respectively. The priority order of the target tasks is shown in table 3, where "Target" denotes the target task number, "P_{FPSM}" denotes the priority of the target task generated using the FPSM, "$P_{MSIMPUE-UA}$" denotes the priority of the target task generated using MSIMPUE-UA.

Figure 8 shows the initial priority analysis of the target tasks using both the MSIMPUE-UA and FPSM methods, where '-*-' denotes the target priority corresponding to each target task and is connected by target task '*' with straight lines of different colors. Fig. 8(a) shows the target priority results of 30 target tasks at the initial moment under the two methods, from which it can be seen that there is a difference in the value of the priority obtained by the same target task in MSIMPUE-UA and FPSM.

Then, we sort the target tasks in ascending order of priority and analyze the impact of MSIMPUE-UA and FPSM on the MSIMPUE observation order. Figure 8(b) shows the corresponding priority of each target task. In order to compare the priority order under the two methods more intuitively, FPSM only uses '-*-' to indicate the target priority corresponding to each target task. As shown in Fig. 8(b), the results of the FPSM target task priority show that multiple target tasks are piled up at the same priority within the priority range [2, 7], making it difficult to further judge the observation order of the satellite for executing the target tasks; The target tasks

TABLE 2. Satellite orbital and payload parameters.

No. Sat	a /(km)	e /(°)	i /(°)	Ω /(°)	ω /(°)	φ /(°)	θ_j /(°)	$st_{\max}$ /(s)	A_j (°)	ω_j /(°/s)	r_j^s /(m)
Sat1	6961	0.004	97.691	105.392	2.737	127.475	5	400	30	0.2	200
Sat2	7043	0.011	97.811	141.397	74.605	94.945	5	400	30	0.2	200
Sat3	7032	0.009	98.134	199.035	232.551	164.415	5	450	30	0.2	200
Sat4	6775	0.010	97.582	319.482	81.116	211.886	5	450	30	0.3	200
Sat5	7062	0.001	98.171	194.922	84.394	275.739	6	500	35	0.3	150
Sat6	7062	0.002	98.230	194.545	92.108	268.029	6	500	35	0.3	150
Sat7	6852	0.002	97.391	244.273	44.203	70.729	6	550	40	0.4	150
Sat8	7127	0.003	98.471	201.257	71.935	288.211	6	550	40	0.4	150

TABLE 3. The results of local area pre-priority setting method and MSIMPUE model based on uncertainty assessment.

Target task prioritization															
Target	T1	T2	T3	T4	T5	T6	T7	T8	T9	T10	T11	T12	T13	T14	T15
P_{FPSM}	8	4	5	4	1	8	8	6	9	4	6	6	8	10	5
$P_{MSIMPUE-UA}$	8.5	5.4	6.1	4.2	0.8	9.7	7.3	5.0	8.1	5.7	7	5.6	8.8	9.5	5.5
Target	T16	T17	T18	T19	T20	T21	T22	T23	T24	T25	T26	T27	T28	T29	T30
P_{FPSM}	7	6	7	8	8	2	8	7	5	4	7	9	6	7	3
$P_{MSIMPUE-UA}$	6.2	5.3	6.6	7.7	7.9	2.8	8.9	7.5	6.3	4.4	6.8	8.4	6.5	6.4	3.4

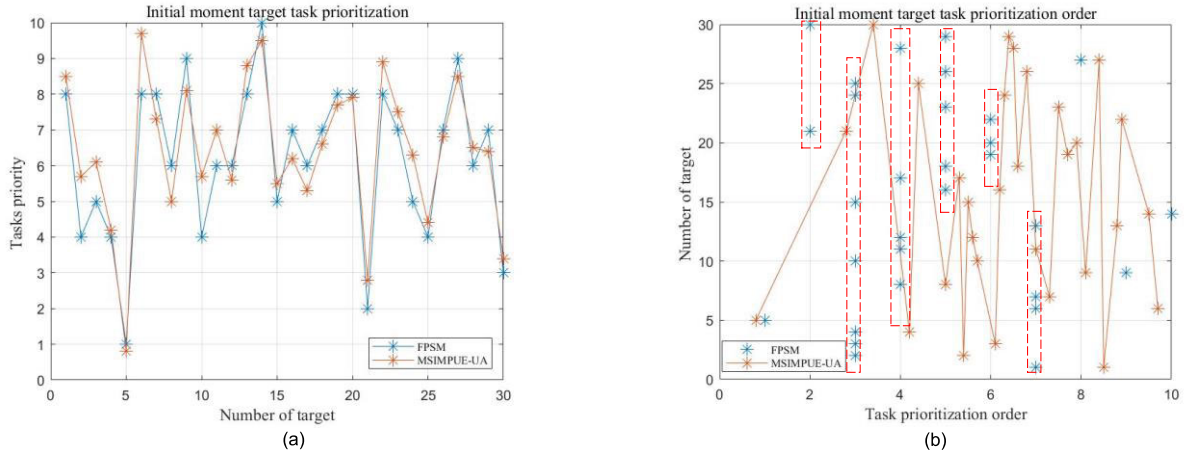

FIGURE 8. The task priority of fixed priority setting method and MSIMPUE model based on uncertainty assessment. (a) The task priority results (b) Target task and the corresponding priority.

using MSIMPUE-UA are uniformly distributed in the range of priority [1, 10], and satellites can be assigned to perform observations of the target tasks in the order of target priority.

At T moment, the Satellite Control Centre monitored the arrival of 10 new missions in the uncertain environment and the change of the target mission at the initial moment: Target task T5, Satellite failure urgently requires new satellites to take over the task of observing major disasters; Target task T7, Reduced cloud cover; Target task T30, Changes in user observation tasks. To cope with the impact of newly arrived missions in an uncertain environment, satellite controllers update the MSIMPUE-UA with indicators such as the urgency of uncertainties and the number of uncertainties contained in a single mission based on actual environmental changes. Figure 9 shows the target task priority information generated by the MSIMPUE-UA and FPSM methods.

Figure 9(a) shows the target priority results for the MSIMPUE-UA and FPSM methods at T time; the red pentagrams and red boxes represent the T5, T17, and T30 target tasks and their related MSIMPUE-UA priorities at the initial and T time, respectively. Figure 9(a) shows that the priority comparison between T5, T17, T30 and the initial moment

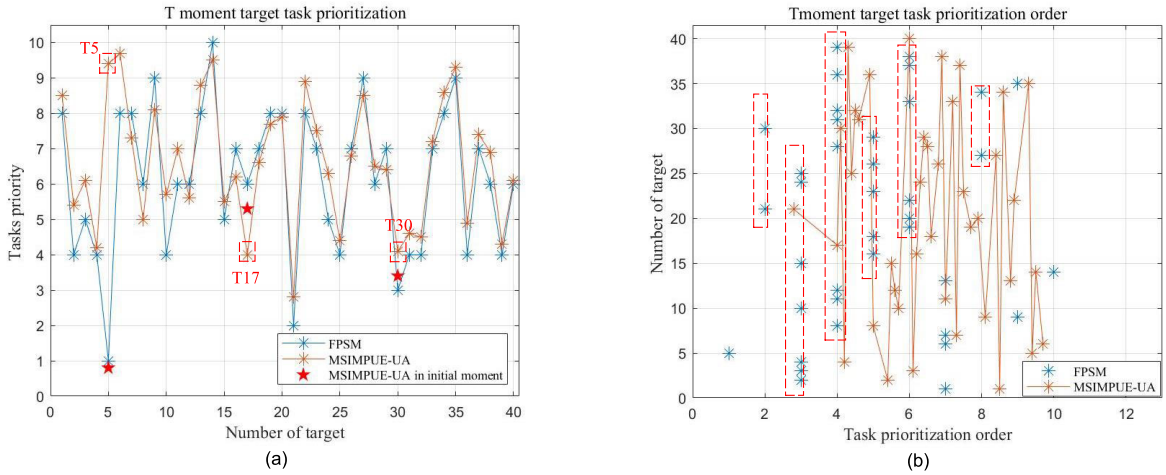

FIGURE 9. T moment, the task priority of fixed priority setting method and MSIMPUE model based on uncertainty assessment. (a) The task priority results (b) Target task and the corresponding priority.

changes, which shows that MSIMPUE-UA is capable of generating a priority for the satellite to perform the target mission that can be dynamically updated according to changes in the uncertain environment.

The corresponding priority of each target task is shown in Figure 9(b), which shows that the FPSM is adopted at the T time, the target tasks appear to be stacked up more obviously, and the new task using MSIMPUE-UA is combined with the target task information of the initial time, and the priority order of the target tasks is fine-tuned compared with that of the initial time, which indicates that the priority of the target tasks generated by MSIMPUE-UA can be updated dynamically according to the change of the uncertain environment.

The simulation results of Experiment 1 show that the MSIMPUE model proposed in this work takes into account the uncertainties in the environment, and dynamically updates the priority order of the target tasks under the uncertain environment, which affects the observation order of the satellite performing the target tasks, and allows the satellite to have more chances to select more important tasks for observation in the process of observation the environment.

C. EXPERIMENT 2: EFFECTIVENESS AND STABILITY OF MSIMPUE WITH SMALL-SCALE NEW TASK INSERTIONS

In this experiment, 30 imaging target locations are randomly produced within the local range of longitude [0, 65] and latitude [0, 150] to imitate the tasks required by users. Figure 10 shows the spatial distribution of the 30 target points observed within the local area.

To validate the effectiveness of the HLRS-MSFADE algorithm in implementing MSIMPUE with small-scale new task insertion, experiments are initially performed to evaluate whether the HLRS-MSFADE algorithm can solve the MSIMPUE's initial task planning scheme.

Table 4 displays the initial mission planning results of the optimal allocation of 30 target tasks using the HLRS-

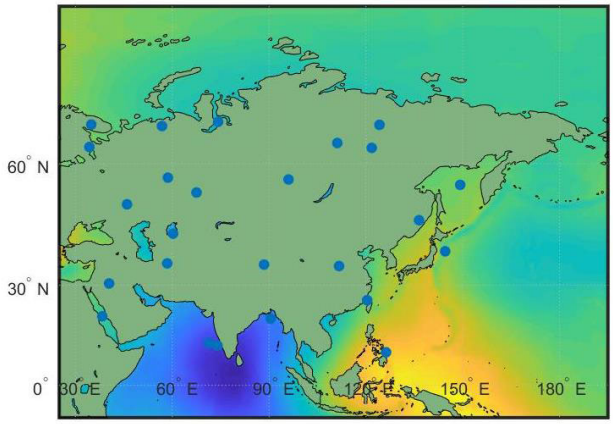

FIGURE 10. Schematic of the distribution of imaging targets in a local area.

MSFADE algorithm. "T" represents the number of target tasks, "S" denotes the satellite number executing the task, "P" represents the target priority, "St" is the observation start time(hour: minute:second), "Et" is the observation end time (hour: minute:second), and "θ_a " is the satellite yaw angle. As shown in the Table 4, all 30 target tasks in this scenario are effectively assigned, and the HLRS-MSFADE algorithm achieves an acceptable mission planning effect.

When implementing the MSIMPUE's initial mission planning scheme, the satellite's mission needs change in an unpredictable environment. On May 8, at 3:00:00, five new tasks arrived, which are analyzed using the MSIMPUE model based on the assessment of uncertain elements. The HLRS is then utilized to perform local replanning of the initial mission planning scheme in an attempt to insert the new mission within the satellite's original observation schedule. Table 5 depicts the MSIMPUE scheme of new task insertion, where new task insertion is represented as T31–T35 in the MSIM-

TABLE 4. Simulated experimental results of local area.

T	S	P	St	Et	θ_a	T	S	P	St	Et	θ_a
T1	S6	6.8	02:31:50	02:31:57	13.93°	T16	S6	7.6	07:50:38	07:50:59	39.45°
T2	S4	5.4	08:28:03	08:28:12	−23.09°	T17	S8	6.4	01:42:31	04:42:52	35.24°
T3	S4	5.7	01:42:36	01:42:49	16.95°	T18	S7	6.1	22:45:33	22:45:53	−35.7°
T4	S2	4.3	07:48:33	07:48:54	−25.30°	T19	S7	6.6	08:04:04	08:04:11	24.84°
T5	S3	4.5	06:22:25	06:22:33	−32.96°	T20	S5	5.5	07:49:41	07:50:02	−36.60°
T6	S4	9.1	02:32:40	02:32:47	13.93°	T21	S1	8.3	07:56:49	07:56:56	44.46°
T7	S7	7.2	09:14:55	09:15:08	−33.16°	T22	S3	6.2	09:37:44	09:37:52	26.78
T8	S3	9.0	06:52:38	09:39:33	14.76°	T23	S7	9.0	06:01:34	06:01:55	38.22°
T9	S3	8.0	09:39:26	09:39:33	−21.40°	T24	S6	8.1	08:27:42	08:27:51	40.00°
T10	S6	6.1	06:21:34	06:22:42	−32.96°	T25	S1	9.7	08:29:06	08:27:51	39.80°
T11	S1	9.7	12:40:31	12:41:11	−36.20°	T26	S5	6.9	23:52:28	23:52:49	−35.9°
T12	S5	4.3	03:01:27	03:01:50	−37.00°	T27	S6	5.4	10:52:09	10:54:21	35.21°
T13	S8	4.5	06:51:40	06:51:50	14.76°	T28	S1	7.5	06:22:23	06:22:30	−38.00°
T14	S2	8.3	18:38:27	18:39:07	−9.29°	T29	S7	7.2	08:28:36	08:28:46	37.84°
T15	S3	8.2	11:09:32	11:10:19	33.51°	T30	S8	6.0	00:21:48	00:22:01	−6.48°

TABLE 5. Simulated experimental results of MSIMPUE for newly arrived task insertion.

NT	S	P	St	Et	θ_a	Insertion method	Perturbation	Mission Benefit
NT1(T31)	S5	7.3	07:44:45	07:44:57	-17.10°	IINCCM	0.5	
NT2(T32)	S6	8.3	06:21:46	06:22:09	-39.43°	SINCCM	0.25	273.60
NT3(T33)	S1	9.0	12:45:50	12:46:14	35.36°	IINCCM	0.5	**Response Time(s)**
NT4(T34)	S3	9.2	11:11:39	11:12:02	39.47°	IIACCM	0.75	
NT5(T35)	S7	4.8	22:46:13	22:46:34	-8.41°	SINCCM	0.25	295.51

PUE scheme, and "Perturbation" indicates the perturbation induced by the insertion of a new task into the initial mission planning scheme.

As shown in Table 5, the new tasks are effectively inserted by using the HLRS, with SINCCM independently inserting two new tasks without conflict cost, and the number of time windows of the original satellite observation sequence is expanded. The two new missions use the IINCCM conflict-free synthetic insertion approach, the number of time windows of the observation sequence of the original satellite remains unchanged, and the imaging time changes. To prevent conflict costs, one new task uses the IIACCM iteration insertion approach, whereas the time frame of the observation sequence syn-thesis task of the original satellite changes.

According to the optimal assignment results of the MSIMPUE scheme shown in Tables 4 and 5, the HLRS-MSFADE algorithm is used to visualize the MSIMPUE simulation results for solving the new task insertion of small-scale tasks to directly represent the assignment relationship between the satellite and the target task, as shown in Figure 11.

Figure 11 demonstrates the efficacy of the HLRS-MSFADE method for solving small-scale mission and inserting new tasks into the MSIMPUE. Figure 11 (a) depicts the results of the HLRS-MSFADE algorithm's initial multi-satellite mission planning scheme, where "*" represents the target task, and the connection of lines "*" with different colors reflects the target task assigned by different satellites. Thirty target tasks are effectively assigned. Figure 11 (b) shows that the task assignment results are connected by arrows from NT1 to NT5 in the order of execution time in three-dimensional space. In addition, five new tasks are successfully inserted, and the initial task planning scheme is effectively allotted.

To further validate the HLRS-MSFADE algorithm's performance in implementing small-scale new task insertion into the MSIMPUE, a simulation experiment is established, in which 10, 15, 20, and 25 new tasks arrive at 3:00 a.m. on May 8, correspondingly, in the same scenario.

Table 6 lists the optimal simulated experimental results of the HLRS-MSFADE algorithm for solving MSIMPUE under different new task scales in Experiment 2. N_{task} represents the number of initial target tasks, N_{ntask} represents the number of new target tasks, N_{insert} represents the number of successful inserts of new tasks, and *Time* is the task response time of MSIMPUE. In this experiment, the experimental results are analyzed with the evaluation indexes.

(1) The successful insertion rate of the new mission is calculated as $R_{insert} = (N_{insert} / N_{ntask}) * 100\%$, which indicates the percentage of successfully inserted new tasks in relation to the total number of new tasks, where $N_{initial}$ is the number of successfully inserted new tasks, and N_{ntask} is the total number of new tasks.

(2) The execution rate of MSIMPUE scheme is calculated as $R_{execute} = \frac{N_{initial}+N_{insert}}{N_{ntask}+N_{task}} * 100\%$, which represents the proportion of tasks completed in the MSIMPUE scheme compared with the total number of tasks, where $N_{initial}$ represents the number of tasks completed in the initial mission planning scheme, and N_{task} denotes the total number of tasks in the original task planning scheme.

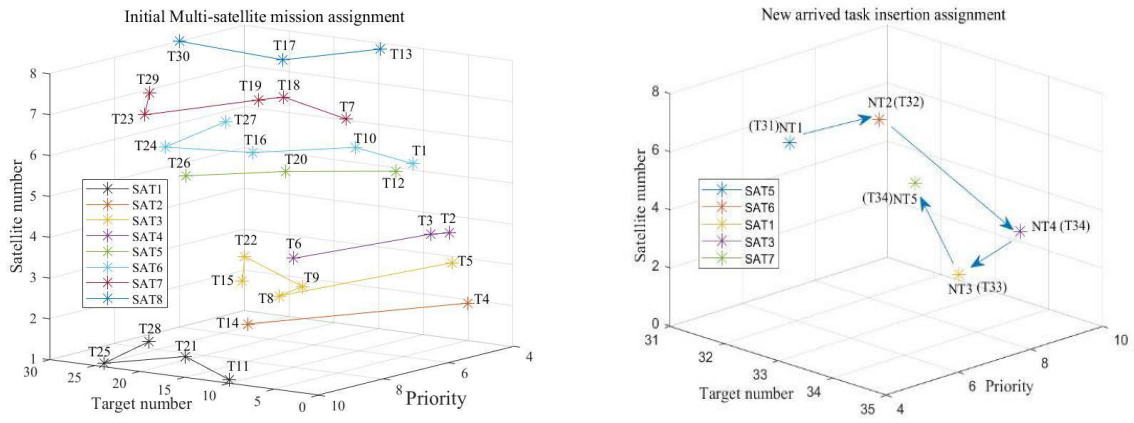

(a) (b)

FIGURE 11. MSIMPUE simulation results for small-scale new task insertion. (a) The result of initial multi-satellite mission assignment; (b) The result of newly arrived task insertion assignment.

TABLE 6. Simulated experimental results of MSIMPUE for newly arrived task insertion.

N_{task}	N_{ntask}	N_{insert}	*Time* (s)	SINCCM	IINCCM	IIACCM	AIMCCM	$I\_benefit$	$M\_benefit$	per_{total}
30	10	10	105.953	4	4	3	1	303.7	294.8	5
	15	14	107.675	5	4	3	2	352.8	339.2	7.5
	20	19	114.160	6	4	5	4	375.2	343.4	11.25

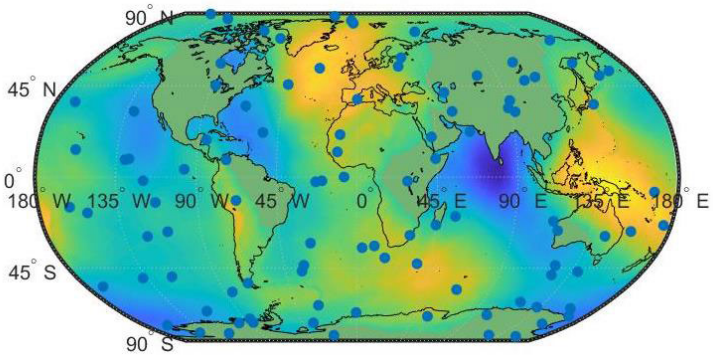

FIGURE 12. Global location distribution of 100 target tasks.

(3) The ideal benefit is calculated as $I\_benefit = \sum_{i=1}^{N_{task}} priority_{task} + \sum_{i=1}^{N_{ntask}} priority_{ntask}$, which represents the sum of the priorities of the target task, assuming that the initial target task and the new task are executed.

(4) The mission benefit is calculated as $M\_benefit = \sum_{i=1}^{N_{task}} x_{ijk} \cdot priority_{task} + \sum_{i=1}^{N_{ntask}} nx_{ijk} \cdot priority_{ntask}$, which represents the sum of task priorities of all target tasks executed by the MSIMPUE scheme.

(5) $per_{total} = \sum_{i=1}^{N_{ntask}} perx_{i,\alpha} \cdot \alpha$ denotes the motion perturbation, which indicates the changes in the satellite observation mission sequence during the entire MSIMPUE process.

The data in Table 6 show that the HLRS-MSFADE algorithm can complete the MSIMPUE inserted by diverse small-scale new tasks with less perturbation while solving the MSIMPUE mission planning scheme with higher mission benefit in response time.

The simulation results of Experiment 2 show that the proposed HLRS-MSFADE algorithm can effectively solve the MSIMPUE model in the small-scale new task insertion scenario, and realize the generation of initial mission planning scheme and the MSIMPUE scheme of new task insertion under uncertain environment. There-

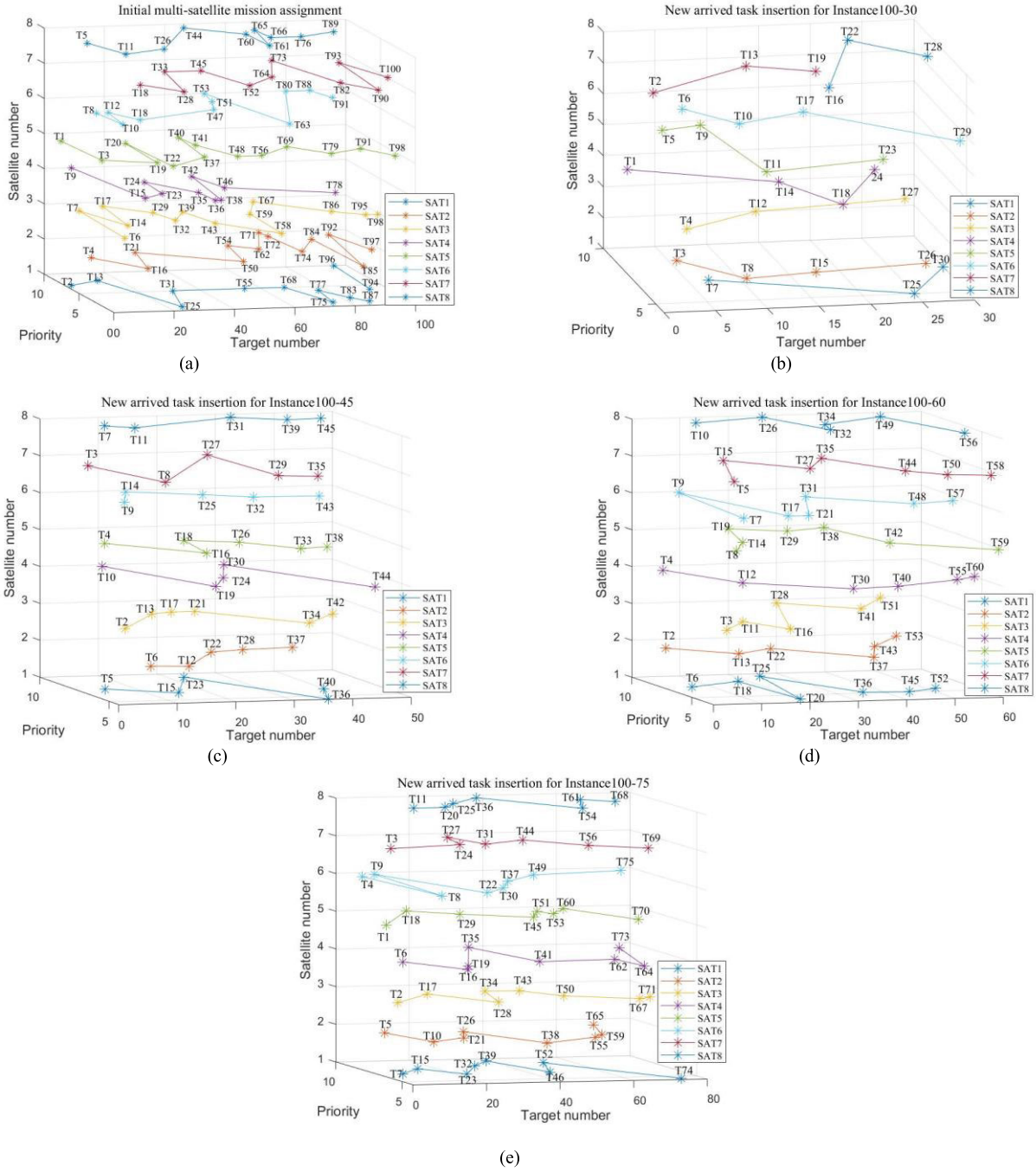

FIGURE 13. Using the HLRS-MSFADE algorithm to solve the initial mission planning scenario, where (a)-(e) is respectively the optimal allocation of the number of new arrivals is 30%, 45%, 60%, and 75% of the initial number of multi-satellite missions.

fore, MSIMPUE-based HLRS-MSFADE algorithm has good feasibility.

D. EXPERIMENT 3: EFFECTIVENESS AND STABILITY OF MSIMPUE WITH LARGE-SCALE NEW TASK INSERTIONS

In Experiment 3, large-scale new tasks are selected and introduced into MSIMPUE to investigate the HLRS-MSFADE algorithm. To replicate the user's imaging task requirements, 100 imaging target task scenarios are randomly produced in the global range of longitude [−90, 90] and latitude [−180, 180]. Figure 12 depicts the global geo-graphical distribution of 100 target tasks. Assume that at 3:00:00 on May 8, large-scale new tasks arrive in batch, with the amounts of new tasks being 30%, 45%, 60%, and 75% of the initial number of multi-satellite tasks. Instances A-B show the simulation example, where A represents the initial number of multi-satellite tasks, and B indicates the number of new tasks.

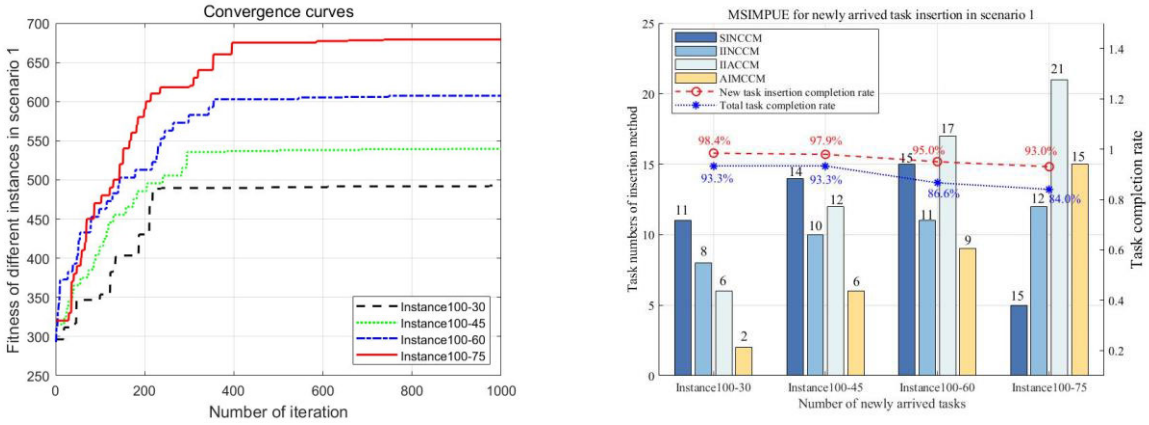

(a) (b)

FIGURE 14. HLRS-MSFADE simulation results for large-scale new task insertion under 100 imaging target task scenarios. (a) convergence curves of MSIMPUE fitness values; (b) statistical graph of synthetic insertion method of various instance.

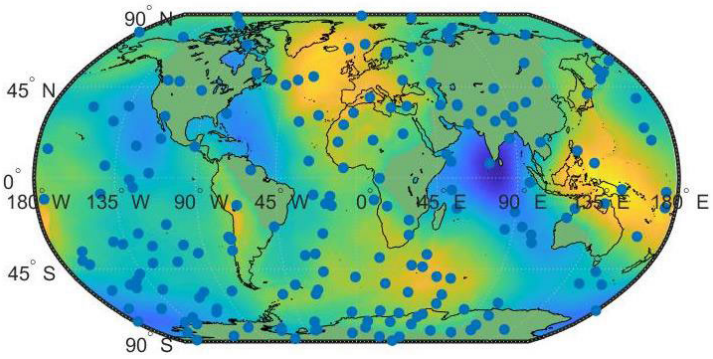

FIGURE 15. Global location distribution of 200 target tasks.

The HLRS-MSFADE algorithm is used to solve large-scale new tasks in MSIMPUE simulation results to directly depict the assignment relationship between the satellite and target tasks. Figure 13 depicts the optimal allocation results, where the number of new tasks solved by the HLRS-MSFADE algorithm for 100 imaging target task scenarios is 30%, 45%, 60%, and 75% of the initial number of multi-satellite tasks. The result of the HLRS-MSFADE algorithm addressing the initial multi-satellite mission planning scheme is shown in Figure 13 (a). Figures 13 (b)–13 (e) depict the optimal allocation results of the HLRS-MSFADE algorithm while solving simulated Instances 100-30, 100-45, 100-60, and 100-75, respectively.

Figure 14 depicts the fitness value and task insertion method performance analysis of large-scale new task insertions in the HLRS-MSFADE algorithm under 100 imaging target task scenarios. Figure 14 (a) depicts the convergence curves of MSIMPUE fitness values for Instances 100-30, 100-45, 100-60, and 100-75 in 100 imaging target task scenarios. Figure 14 (b) shows the statistical graph of synthetic insertion method of In-stances 100-30, 100-45, 100-60, and 100-75 solved by the HLRS-MSFADE algorithm.

The convergence curves of the fitness values of Instances 100-30, 100-45, 100-60, and 100-75 have a similar convergence trend, as illustrated in Figure 14(a). The number of new tasks is determined, and the fitness values rise significantly. In the first 400 generations, all of them converge to the ideal solution, demonstrating that the HLRS-MSFADE algorithm has good convergence performance.

Figure 14(b) depicts the use of the four insertion options in the HLRS, as well as the successful insertion rate of new tasks and the MSIMPUE scheme implementation rate in 100 imaging target task scenarios. The figure shows that the four task insertion methods in the hybrid local replanning approach achieve dynamic insertion of new tasks in four instances, Instance100-30, Instance100-45, Instance100-60, and Instance100-75, and the successful insertion rate of new tasks exceeds 90%. Furthermore, the execution rate of the MSIMPUE scheme in instances Instance100-60 and Instance100-70 decreases significantly as the target task numbers increase.

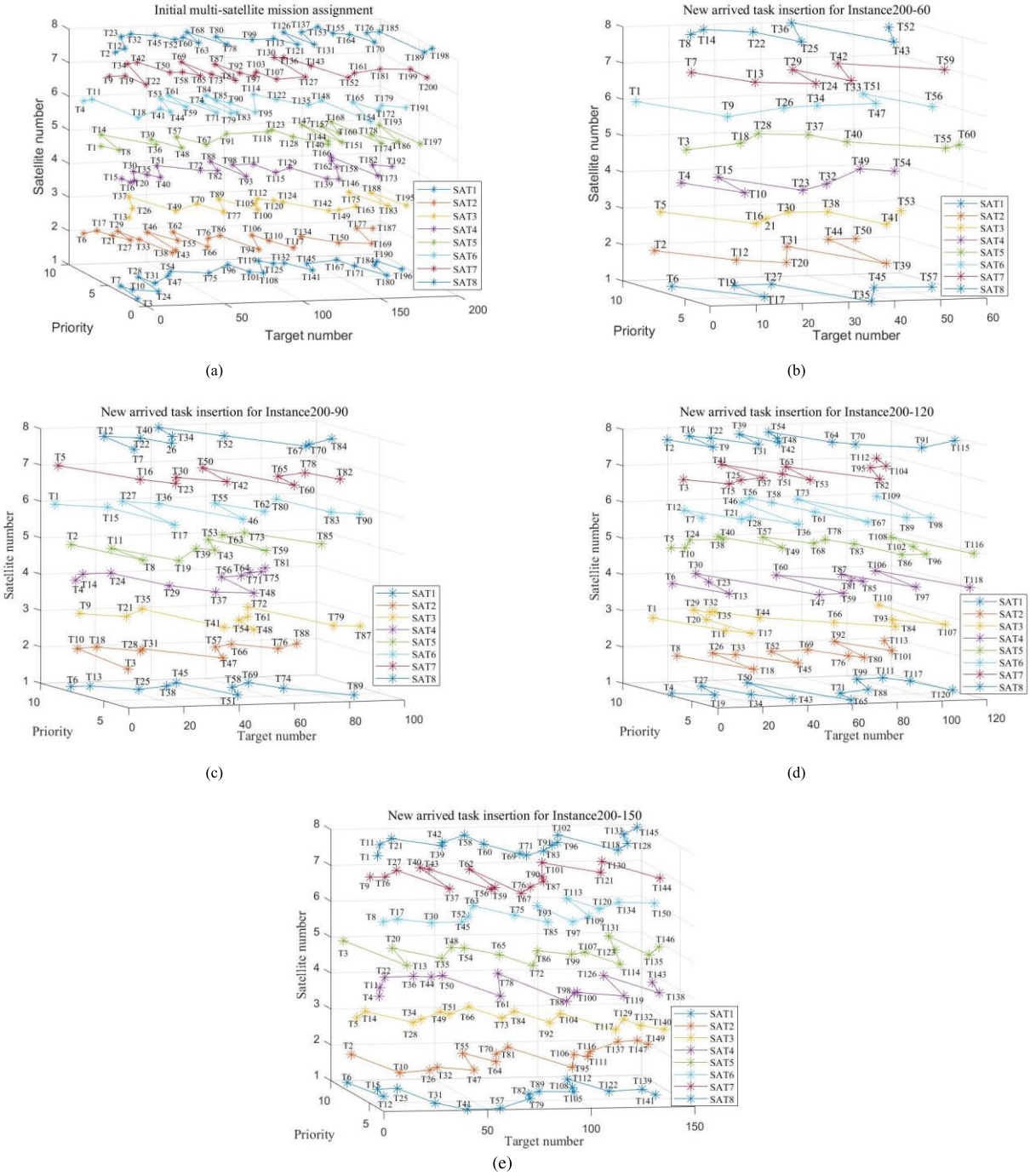

FIGURE 16. Using the HLRS-MSFADE algorithm to solve the initial mission planning scenario, where (a)-(e) is respectively the optimal allocation of the number of new arrivals is 30%, 45%, 60%, and 75% of the initial number of multi-satellite missions.

This part randomly produces 200 imaging target tasks within the same latitude and longitude range and simulation time to imitate the user's imaging task needs, further validating the stability of the HLRS-MSFADE method by using MSIMPUE to verify large-scale new tasks. Figure 15 depicts the global geographical distribution of 200 target tasks.

The optimal assignment results of multiple newly inserted tasks under the HLRS-MSFADE algorithm in 200 imaging target task scenarios are shown in Figure 16.

Figure 17 depicts the performance study of repeated new task insertions of the HLRS-MSFADE algorithm in two aspects of fitness value and task insertion method under 200 imaging target task scenarios.

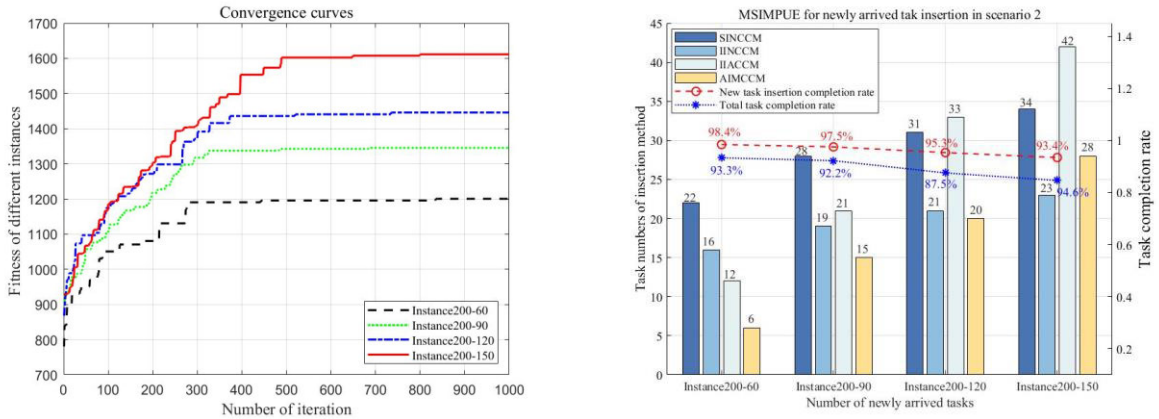

(a) (b)

FIGURE 17. MSIMPUE simulation results for large-scale new task insertion under 200 imaging target task scenarios. (a) convergence curves of MSIMPUE fitness values; (b) statistical graph of synthetic insertion method of various instance.

As shown in Figure17 (a), as the number of new tasks increases, the convergence speed of the HLRS-MSFADE algorithm decreases, but it can still solve the best allocation scheme within the effective number of iterations. Figure17 (b) demonstrates that the HLRS-MSFADE algorithm can realize dynamic task insertion. Furthermore, in Instances 200-60 and 200-90, the task insertion mode is SINCCM > IINCCM > IIACCM > AIMCCM. The reason is that the number of new tasks is small when it accounts for 30%–45% of the initial multi-satellite tasks, and most of the new tasks can insert the satellite observation sequence using the insertion method without conflict loss. When the number of new tasks accounts for 60% of the initial multi-satellite tasks, the proportion of new tasks is extremely high, and the time window resources are limited, as are the tasks that may be arranged. The adoption of AIMCCM and IIACCM has increased.

The MSIMPUE data from 100 and 200 imaging target task scenarios in an uncertain environment are counted. Table 7 displays the total tasks of the initial mission planning scheme N_{task}, the number of new target tasks N_{ntask}, the number of successful task insertions N_{insert}, ideal benefit $I\_benefit$, mission benefit $M\_benefit$, response time $Time$, motion perturbation per_{total}, the successful insertion rate of new tasks R_{insert}, and the execution rate of the MSIMPUE scheme $R_{execute}$.

The results presented in Table 7 show that the response time increases with the new task scale; however, MSIMPUE issues with various new task scales can still be solved with high mission benefit and low motion perturbation.

The simulation results of Experiment 3 show that the proposed HLRS-MSFADE algorithm can effectively address the assignment relationship between many new tasks inserted into the MSIMPUE satellite and the target tasks. Therefore, the MSIMPUE-based HLRS-MSFADE algorithm has good stability.

E. EXPERIMENT 4: HLRS-MSFADE ALGORITHM PERFORMANCE ANALYSIS

To verify the performance of the HLRS-MSFADE algorithm in solving MSIMPUE further, its effectiveness is discussed in this section. Subsequently, its performance is compared with that of other similar algorithms. Finally, HLRS-MSFADE algorithm performance is compared with other similar algorithms.

1) COMPARISON EXPERIMENT OF DIFFERENT MUTATION STRATEGIES IN HLRS-MSFADE ALGORITHM

Large-scale examples are more likely to reflect the performance of the HLRS-MSFADE algorithm in solving MSIMPUE. We compare the search capabilities of various differential crossover strategies under new arrival task Instances 200-60, 200-90, 200-120, and 200-150.

As shown in Figure 18, the performance of the HLRS-MSFADE algorithm can be analyzed from three aspects.

First, fusion mutation strategies converge to near-optimal solutions faster than single mutation strategies, reducing the scale of random search and greatly improving algorithm performance. This finding indicates that the HLRS-MSFADE algorithm quickly guides the search toward the global optimal. Second, the optimal solution of the current population found by the HLRS-MSFADE algorithm is of higher quality, as the fusion mutation method improves population diversity. Finally, the convergence curves of the four groups of new task instances show that the algorithm still has a convergence process in the middle and late stages of evolution. Thus, the combined action of dynamic crossover rate and fusion mutation strategy in the HLRS-MSFADE algorithm can effectively balance the algorithm's explosiveness and exploration and prevent it from falling into the local optimal.

TABLE 7. Assignment results of performance analysis in Scenarios 1 and 2.

Scenario	N_{task}	N_{ntask}	N_{insert}	*Time* (s)	$I\_benefit$	$M\_benefit$	per_{total}	R_{insert}	$R_{execute}$
100 imaging target task scenarios	100	30	28	338.455	860.9	842.4	14.25	93.3%	98.4%
		45	42	365.144	961.1	942.2	23.5	93.3%	97.9%
		60	52	384.254	1071.6	1018.1	31.0	86.6%	95.0%
		75	63	430.780	1187.4	1100.8	44.77	84.0%	93.0%
200 imaging target task scenarios	200	60	56	472.530	1728.5	1696.6	28.5	93.3%	98.4%
		90	83	501.196	1973.4	1925.9	47.25	92.2%	97.5%
		120	105	533.061	2155.1	2041.9	63.0	87.5%	95.3%
		150	127	541.893	2389.9	2229.9	75.75	84.6%	93.4%

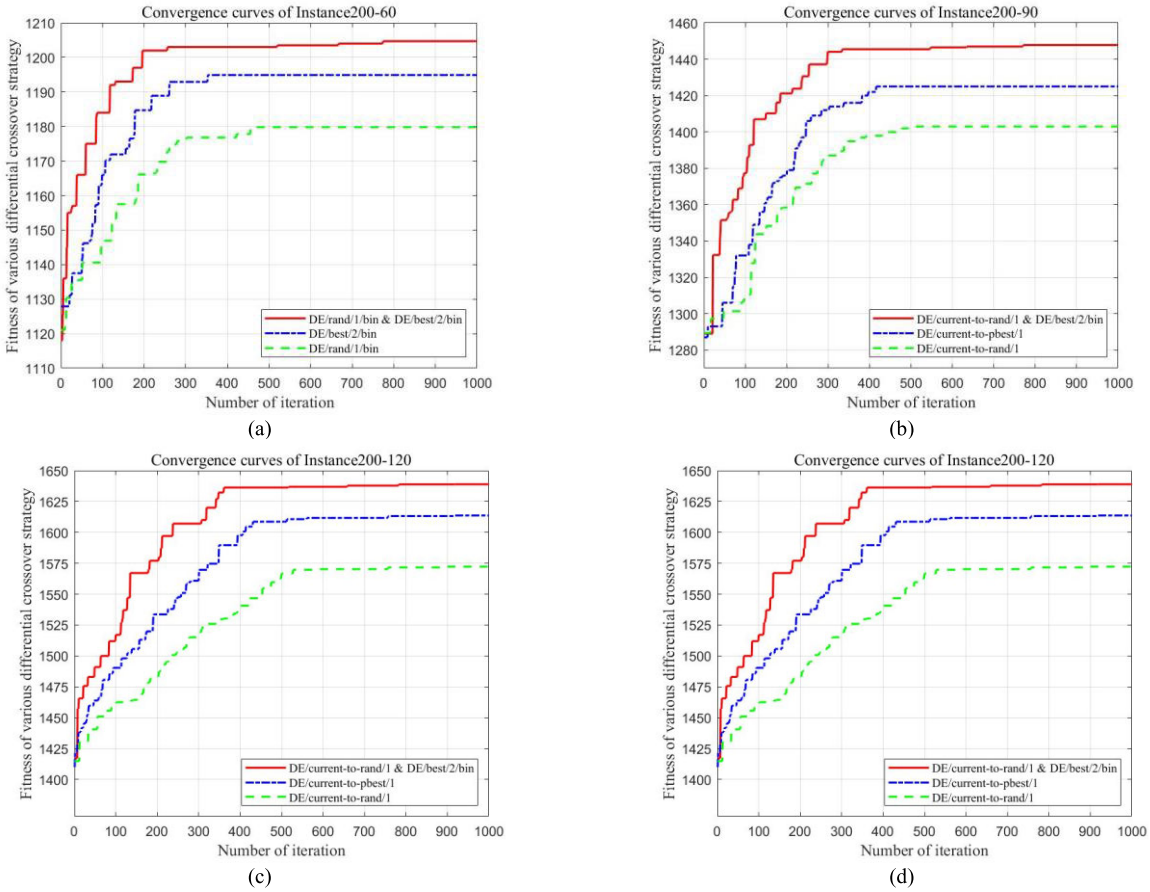

FIGURE 18. Fitness convergence curves for various differential crossover strategies, where (a)-(d) is respectively the con convergence curves of Instance200-60, Instance200-90, Instance200-120, Instance200-120 in differential crossover strategies.

2) PERFORMANCE COMPARISON EXPERIMENT BETWEEN HLRS AND FIA

We carry out a performance comparison experiment between the HLRS-MSFADE algorithm's hybrid local replanning strategy (HLRS) and the ISAH-FIA algorithm's fast insertion approach (FIA), where the experimental scenarios are randomly set up with 100 target task scenarios and 200 target task scenarios with insertion of 30%, 45%, 60%, and 75% of the new arriving task instances, and the simulation instances are denoted by Instance A-B, where A denotes the number of target task instances. The experimental results of the performance comparison between HLRS and FIA are shown in Table 8 and Figure 19.

The performance evaluation of multi-satellite imaging mission planning in uncertain environments using HLRS with FIA is recorded in Table 8. In Table 8 displays the number of successful task insertions N_{insert}, ideal benefit $I\_benefit$, mission benefit $M\_benefit$, response time *Time*, motion perturbation per_{total}, the successful insertion rate of new tasks R_{insert}, and the execution rate of the MSIMPUE scheme $R_{execute}$, In order to comprehensively evaluate the effectiveness of HLRS and FIA on the MSIMPUE problem, Figure 19

TABLE 8. MSIMPUE simulation results of different instances by using insertion method.

Instances	*I_benefit*	Hybrid Local Replanning Strategy (HLRS)						Fast insertion method (FIA)					
		N_{insert}	$Time(\mathbf{s})$	per_{total}	*M_benefit*	R_{insert}	$R_{execute}$	N_{insert}	$Time(\mathbf{s})$	per_{total}	*M_benefit*	R_{insert}	$R_{execute}$
100-30	860.9	28	338.455	14.25	842.4	93.3%	98.4%	27	400.451	20.25	819.6	90.0%	97.60%
100-45	961.1	42	365.144	23.50	942.2	93.3%	97.9%	38	423.753	28.50	852.3	84.4%	95.17%
100-60	1071.6	52	384.254	31.00	1018.1	86.6%	95.0%	42	472.956	36.75	927.2	70.0%	88.75%
100-75	1187.4	63	430.780	44.77	1100.8	84.0%	93.0%	49	507.845	47.75	961.2	65.4%	85.14%
200-60	1728.5	56	472.530	28.50	1696.6	93.30%	98.4%	53	598.783	39.75	1644.7	88.3%	97.30%
200-90	1973.4	83	501.196	47.25	1925.9	92.20%	97.5%	74	621.794	68.50	1794.6	82.2%	94.48%
200-120	2155.1	105	533.061	63.00	2041.9	87.5%	95.3%	85	647.162	80.75	1837.8	70.8%	89.06%
200-150	2389.9	127	541.893	75.75	2229.9	84.6%	93.4%	94	701.218	88.20	1924.3	62.6%	84.00%
Avg	1540.98	69	445.9	41.00	1474.7	89.3%	96.1%	57	545.495	51.30	1345.2	76.7%	91.44%

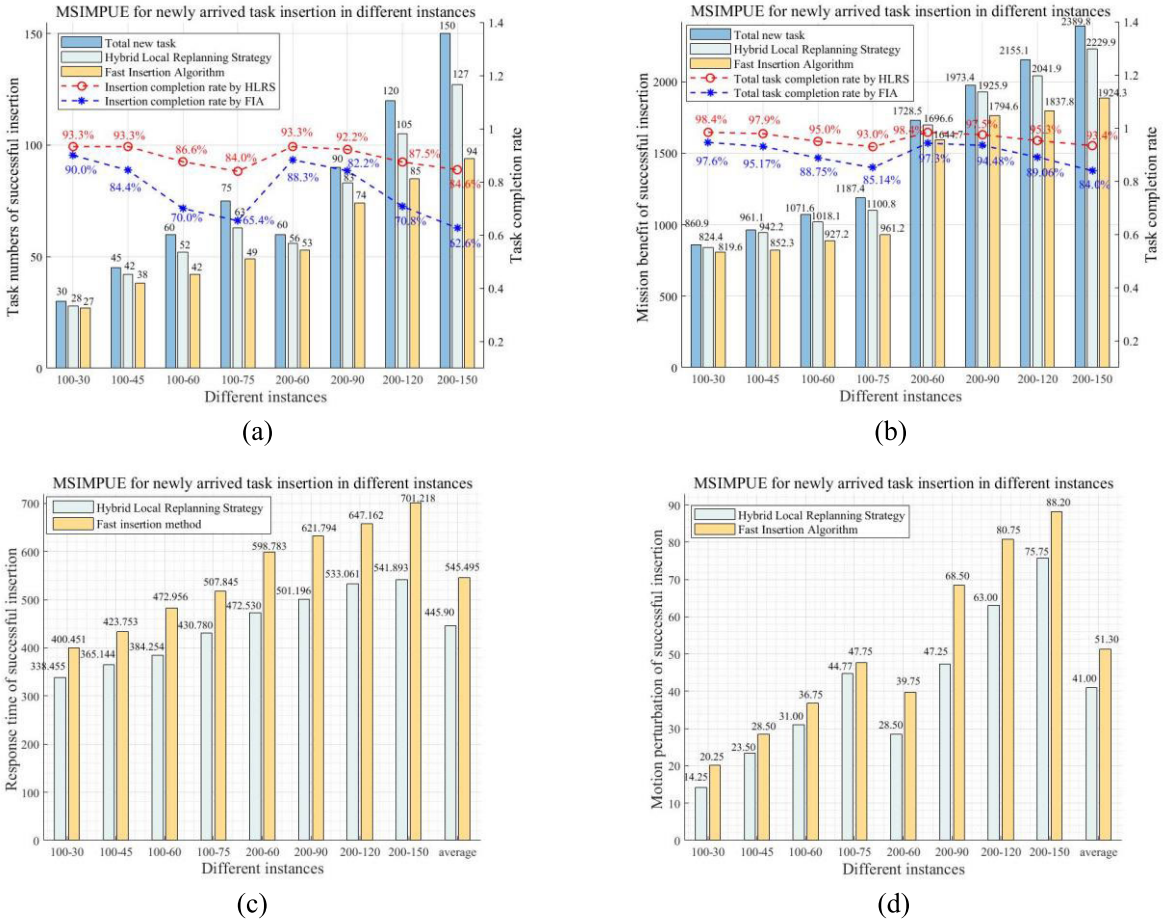

FIGURE 19. Results of experiments comparing the performance of the hybrid local replanning strategy and fast insertion algorithm. (a) Task numbers of successful insertion; (b) Mission benefit of successful insertion;(c) Response time of successful insertion; (d) Motion perturbation of successful insertion.

shows the visual analysis of the two types of methods in terms of four aspects: the number of successful new task insertions, the target task benefits, the response time and the action perturbations.

According to the experimental results in Table 8 and Figure 19, when the proportion of the new task size to the total number of tasks is small, as in instances Ins100-30 and Ins200-60, both HLRS and FIA can achieve higher target task gains with smaller time responses and smaller action perturbations. This is due to the fact that when the proportion of new mission size to the total number of missions is small, there are more spare resources in the satellite observation

TABLE 9. MSIMPUE simulation results of various instances using different algorithms.

Instances	HLRS-MSFADE				APPDE				MMED			
	$f_{\max}$	f_{avg}	$f_{\min}$	$std.$	$f_{\max}$	f_{avg}	$f_{\min}$	$std.$	$f_{\max}$	f_{avg}	$f_{\min}$	$std.$
100-30	494.4	490.2	483.9	4.3	465.8	455.6	452.3	5.74	420.5	413.4	400.1	8.5
100-45	559.3	553.1	545.8	5.5	500.8	493.1	477.2	9.8	475.4	472.2	452.7	10.0
100-60	612.8	603.6	596.2	6.8	593.8	576.3	562.0	13.1	575.7	561.2	545.1	12.4
100-75	632.2	622.1	616.3	6.6	618.1	602.3	581.4	15.0	606.8	588.8	574.7	13.1
200-60	1203.2	1195	1185.3	7.3	1180.2	1158	1143.3	15.2	1083.9	1063.8	1051.9	13.2
200-90	1455.7	1444.6	1435.4	8.3	1290.8	1271.3	1250.3	16.5	1195.4	1180.2	1159.8	14.6
200-120	1597.7	1585.3	1578.1	8.1	1419.2	1406.7	1382.8	15.1	1265.7	1281.9	1302.4	15.0
200-150	1631.1	1615.3	1604.7	10.8	1619.4	1589.7	1581.1	16.4	1520.1	1509.2	1480.4	16.7
Avg	1023.3	1013.7	1005.7	7.2	961.0	944.1	928.8	13.3	892.9	883.8	870.9	12.9
Instances	TADE_DDS				FIA				RARA			
	$f_{\max}$	f_{avg}	$f_{\min}$	$std.$	$f_{\max}$	f_{avg}	$f_{\min}$	$std.$	$f_{\max}$	f_{avg}	$f_{\min}$	$std.$
100-30	404.5	395.9	379.4	10.4	398.9	387.8	380.3	7.6	381.3	374.1	359.2	9.2
100-45	470.1	455.3	433.8	14.9	419.7	400.04	389.3	8.7	391.7	385.5	367.5	10.2
100-60	543.9	529.9	506.8	15.2	420.6	417.5	393.2	12.3	409.1	390.9	380.8	11.7
100-75	582.5	560.3	542.2	16.5	467.7	445.6	405.6	13.3	431.8	414.7	398.6	13.5
200-60	1015.4	997.5	974.8	16.6	1007.2	993.5	978.8	11.6	998.1	974.0	963.8	14.3
200-90	1200.8	1177.8	1160.4	16.6	1120.4	1104.3	1086.5	13.9	1109.6	1082.7	1071.6	15.9
200-120	1283.1	1276.5	1243.7	17.2	1146.5	1133.0	1109.8	15.2	1130.0	1111.3	1088.8	16.8
200-150	1493	1455.7	1453.3	18.2	1170.6	1134.8	1129.2	18.3	1162.1	1151.1	1120.3	17.6
Avg	874.2	856.1	836.8	15.7	768.9	752.1	734.1	12.6	751.7	735.5	718.8	13.7

sequence, and the insertion method without conflict loss in FIA and HLRS can be used for new mission insertion by judging the position of mission neighbors.

The use of FIA for new task insertion by judging simply the position of task adjacencies leads to the problem of long response time and a sharp decline in the number of successfully inserted new tasks as the size of new tasks increases as a proportion of the total number of tasks. Furthermore, as new tasks are inserted one by one, there is a scarcity of spare resources in the satellite observation sequence's neighboring position, and the advent of overlapping new missions is a huge perturbation to the satellite observation sequence.

The use of HLRS can thoroughly consider the adjacent positions where the tasks and contained meta-tasks are situated, make full use of the spare satellite resources, reasonably select the insertion positions of new tasks, and achieve more new task insertions in a shorter time. MSIMPUE with HLRS has a considerable advantage over MSIMPUE with FIA in terms of the number of task insertions, mission benefit, response time, and action perturbations.

In conclusion, HLRS with larger new mission scale instances has the advantage over FIA for most cases and can adapt to the multi-satellite imaging mission planning problem in uncertain environments.

3) PERFORMANCE COMPARISON BETWEEN HLRS-MSFADE ALGORITHM AND OTHER ALGORITHMS

The HLRS-MSFADE method is compared with APPDE algorithm (Differential Evolution algorithm based on Accompanying Population and Piecewise) are presented strategy) [32], MMED algorithm (Modified Maximum Extension Distance) [33], TADE_DDS algorithm (Two-Stage Adaptive Differential Evolution with a Dynamic Dual-populations Strategy) [34], FIA Algorithm (Fast Insertion Algorithm) [23], RARA algorithm (Rolling Horizon Based Replanning Algorithm) [15].

The APPDE algorithm uses a concomitant population of stored suboptimal solutions to increase population diversity and is able to improve the diversity of multi-satellite mission planning scenarios in uncertain environments. The MMED algorithm uses the adjustment of the maximum extension distance as a metric to improve the diversity of planning solutions and the efficiency of the solution at different phases of optimization. The TADE_DDS algorithm designs a dynamic

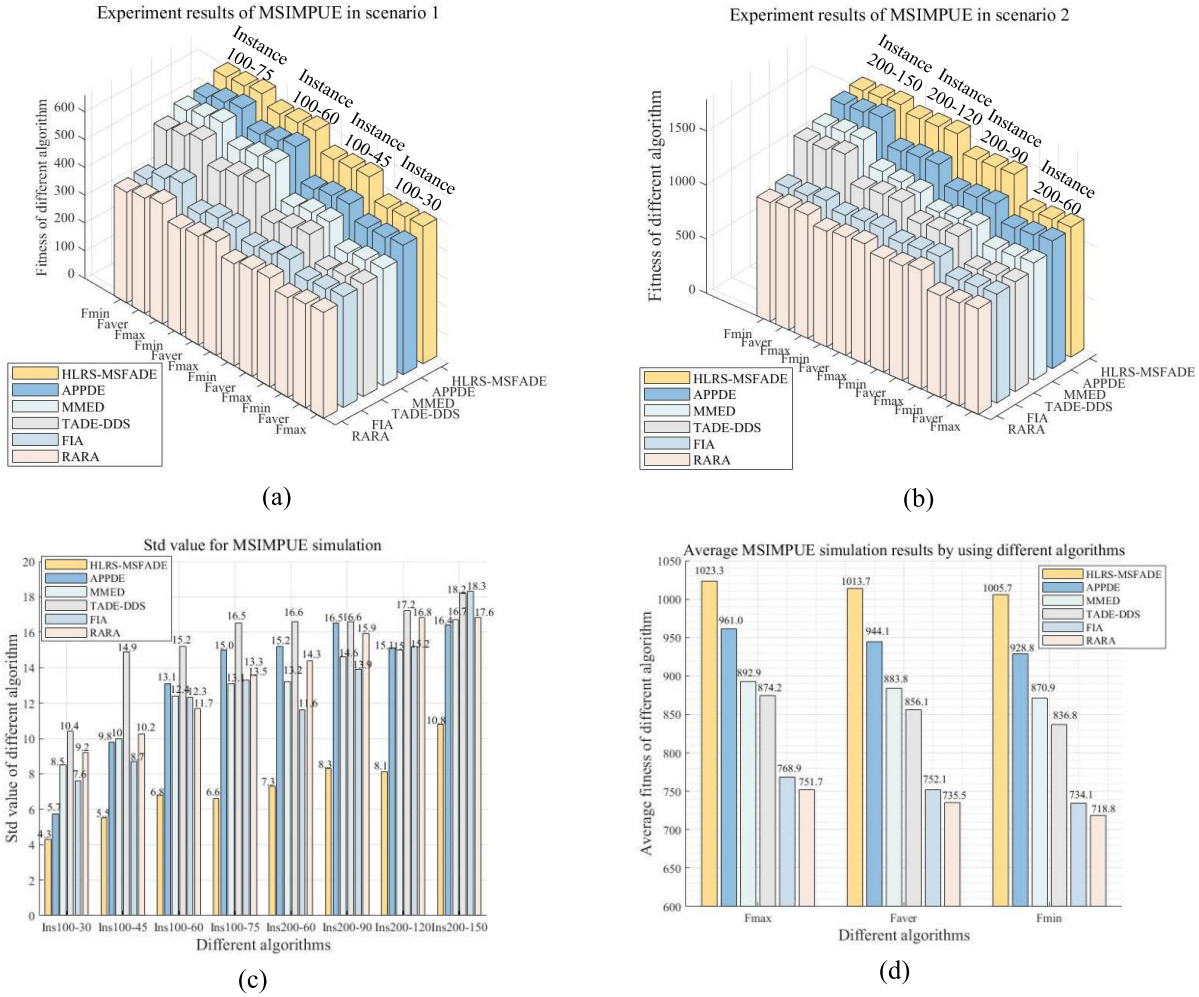

FIGURE 20. Results of experiments comparing the performance of the HLRS-MSFADE algorithm to that of other algorithms. (a)Optimal fitness value, average fitness value, worst fitness value in Instances 100-30, 100-45, 100-60, and 100-75; (b)Optimal fitness value, average fitness value, worst fitness value in Instance200-60, 200-90, 200-120, 200-120.

population strategy that is capable of finding more globally optimal task planning solutions. The FIA algorithm is able to prioritize target tasks with high task gains by judging two adjacent tasks in the satellite observation sequence for new task insertion, which improves the task benefit. The RARA algorithm performs multi-satellite imaging mission replanning for each fixed time interval, fully accounting for multi-satellite mission planning constraints in dynamic environments, and moves back and forth along the time axis to find suitable insertion positions, improving the accuracy of the multi-satellite imaging mission planning scheme.

The experiment used the same number of iterations, population size, and evolution parameters as the previous experiments, and the experimental scenario is the same as inserting 30%, 45%, 60%, and 75% new tasks instances in the 100 and 200 target task scenarios. Table 9 and Figure 20 exhibit the experimental findings of a performance comparison between the HLRS-MSFADE method and other algorithms.

To comprehensively evaluate the effect of HLRS-MSFADE algorithm on the MSIMPUE problem, the optimal fitness value $f_{\max}$, average fitness value f_{avg}, worst fitness value $f_{\min}$, and standard deviation std. are used as evaluation indexes. Table 9 and Figure 20 show that the experimental results of the HLRS-MSFADE algorithm and the comparison algorithms differ significantly. In the optimal fitness value $f_{\max}$, average fitness value f_{avg}, and worst fitness value $f_{\min}$ of eight groups of instances in the 100 and 200 imaging target task scenarios, the HLRS-MSFADE algorithm outperforms the other algorithms, and the fitness value has obvious advantages.

Furthermore, as the number of target tasks increases, the APPDE, MMED, TADE_DDS, FIA and RARA algorithms exhibit noticeable oscillations, whereas the standard deviation of the HLRS-MSFADE algorithm is always lower than those of the other three algorithms. The results show that even as the number of target tasks increases, the HLRS-MSFADE algorithm maintains acceptable stability. In addition, from

Figure 20(a) and Figure 20(b), it can be seen that the FIA algorithm and the RARA algorithm solving the instances with a larger proportion of new task number to the total number of tasks have a smaller difference in fitness values than the instances ins100-45 and ins200-90, which suggests that the FIA algorithm and the RARA algorithm may be trapped in a local optimum. When combined with the experimental analysis in Table 8, it is clear that merely analyzing the neighboring missions of a satellite observation sequence the effect is unsatisfactory for solving the MSIMPUE problem when the size of the new mission is a large proportion of the total number of missions. Generally, the HLRS-MSFADE algorithm outperforms the other algorithms in terms of optimization ability and stability over numerous iterations, and it can adapt to large-scale MSIMPUE environments.

The simulation results of Experiment 4 show that the proposed HLRS-MSFADE algorithm's dynamic crossover rate and fusion mutation strategy can improve population diversity, effectively balance the algorithm's development and exploration, and prevent the algorithm from falling into the local optimum. In terms of convergence speed and fitness value, the HLRS-MSFADE method outperforms the other five algorithms. As a result, employing the HLRS-MSFADE algorithm to solve the MSIMPUE problem has some advantages.

VI. CONCLUSION AND FUTURE WORK

In this work, an MSIMPUE model based on uncertainty assessment is proposed to provide a reasonable basis for MSIMPUE assignment. An HLRS for an uncertain environment is proposed for the first time to address the changing mission requirements in an uncertain environment, which achieves the transformation of the MSIMPUE problem into a new mission insertion problem through the adjustment of the time window between the new mission and the original satellite observation sequence in an uncertain environment. Furthermore, to address the problem of long mission response time and low mission completion rate caused by the MSIMPUE's large solving space and numerous constraints, an MSFADE algorithm is proposed to obtain high-quality MSIM-PUE schemes in a reasonable computing time. The simulation results indicate that the proposed solution can successfully solve the MSIMPUE problem and has outstanding performance in terms of task reaction time and completion rate.

Future research will focus on considering the problem of Human-computer interaction based on MSIMPUE. The algorithm proposed in this work can effectively deal with the MSIMPUE; However, during the actual collaborative mission execution process, the mission requirements present preference, complexity, and conflict, and it has become an intrinsic demand and development trend to introduce Human-computer interaction into MSIMPUE, share MSIM-PUE with the system for solving the preference requirements, receive feedback, and guide the multi-satellite imaging mission planning system to generate the multi-satellite imaging mission planning scheme.

REFERENCES

[1] C. He, Y. Dong, H. Li, and Y. Liew, "Reasoning-based scheduling method for agile earth observation satellite with multi-subsystem coupling," *Remote Sens.*, vol. 15, no. 6, p. 1577, Mar. 2023, doi: 10.3390/rs15061577.

[2] H. Kim and Y.-K. Chang, "Optimal mission scheduling for hybrid synthetic aperture radar satellite constellation based on weighting factors," *Aerosp. Sci. Technol.*, vol. 107, Dec. 2020, Art. no. 106287, doi: 10.1016/j.ast.2020.106287.

[3] J. Long, S. Wu, X. Han, Y. Wang, and L. Liu, "Autonomous task planning method for multi-satellite system based on a hybrid genetic algorithm," *Aerospace*, vol. 10, no. 1, p. 70, Jan. 2023, doi: 10.3390/aerospace10010070.

[4] R. Liu, X. Ding, W. Wu, and W. Guo, "Distributed coordination of space–ground multiresources for remote sensing missions," *Remote Sens.*, vol. 15, no. 13, p. 3362, Jun. 2023, doi: 10.3390/rs15133362.

[5] W. Qiu, C. Xu, Z. Ren, and K. L. Teo, "Scheduling and planning framework for time delay integration imaging by agile satellite," *IEEE Trans. Aerosp. Electron. Syst.*, vol. 58, no. 1, pp. 189–205, Feb. 2022, doi: 10.1109/TAES.2021.3098101.

[6] J. Wang, E. Demeulemeester, X. Hu, and G. Wu, "Expectation and SAA models and algorithms for scheduling of multiple earth observation satellites under the impact of clouds," *IEEE Syst. J.*, vol. 14, no. 4, pp. 5451–5462, Dec. 2020, doi: 10.1109/JSYST.2019.2961236.

[7] X. Han, M. Yang, S. Wang, and T. Chao, "Continuous monitoring scheduling for moving targets by Earth observation satellites," *Aerosp. Sci. Technol.*, vol. 140, Sep. 2023, Art. no. 108422, doi: 10.1016/j.ast.2023.108422.

[8] Z. E., R. Shi, L. Gan, H. Baoyin, and J. Li, "Multi-satellites imaging scheduling using individual reconfiguration based integer coding genetic algorithm," *Acta Astronautica*, vol. 178, pp. 645–657, Jan. 2021, doi: 10.1016/j.actaastro.2020.08.041.

[9] K. Wu, D. Zhang, Z. Chen, J. Chen, and X. Shao, "Multi-type multi-objective imaging scheduling method based on improved NSGA-III for satellite formation system," *Adv. Space Res.*, vol. 63, no. 8, pp. 2551–2565, Apr. 2019, doi: 10.1016/j.asr.2019.01.006.

[10] B. Du and S. Li, "A new multi-satellite autonomous mission allocation and planning method," *Acta Astronautica*, vol. 163, pp. 287–298, Oct. 2019, doi: 10.1016/j.actaastro.2018.11.001.

[11] Q. Luo, W. Peng, G. Wu, and Y. Xiao, "Orbital maneuver optimization of earth observation satellites using an adaptive differential evolution algorithm," *Remote Sens.*, vol. 14, no. 9, p. 1966, Apr. 2022, doi: 10.3390/rs14091966.

[12] Y. Chen, J. Lu, R. He, and J. Ou, "An efficient local search heuristic for earth observation satellite integrated scheduling," *Appl. Sci.*, vol. 10, no. 16, p. 5616, Aug. 2020, doi: 10.3390/app10165616.

[13] Y. Song, J. Ou, J. Wu, Y. Wu, L. Xing, and Y. Chen, "A cluster-based genetic optimization method for satellite range scheduling system," *Swarm Evol. Comput.*, vol. 79, Jun. 2023, Art. no. 101316, doi: 10.1016/j.swevo.2023.101316.

[14] Y. Song, L. Xing, and Y. Chen, "Two-stage hybrid planning method for multi-satellite joint observation planning problem considering task splitting," *Comput. Ind. Eng.*, vol. 174, Dec. 2022, Art. no. 108795, doi: 10.1016/j.cie.2022.108795.

[15] Y. Gu, C. Han, Y. Chen, and W. W. Xing, "Mission replanning for multiple agile earth observation satellites based on cloud coverage forecasting," *IEEE J. Sel. Topics Appl. Earth Observ. Remote Sens.*, vol. 15, no. 5, pp. 594–608, May 2022, doi: 10.1109/JSTARS.2021.3135529.

[16] Z. Li and X. Li, "A multi-objective binary-encoding differential evolution algorithm for proactive scheduling of agile Earth observation satellites," *Adv. Space Res.*, vol. 63, no. 10, pp. 3258–3269, May 2019, doi: 10.1016/j.asr.2019.01.043.

[17] X. Chen, G. Reinelt, G. Dai, and M. Wang, "Priority-based and conflict-avoidance heuristics for multi-satellite scheduling," *Appl. Soft Comput.*, vol. 69, pp. 177–191, Aug. 2018, doi: 10.1016/j.asoc.2018.04.021.

[18] S. E. Ayana and H.-D. Kim, "Optimal scheduling of imaging missions for multiple satellites using linear programming model," *Int. J. Aeronaut. Space Sci.*, vol. 24, no. 2, pp. 559–569, Apr. 2023, doi: 10.1007/s42405-022-00543-7.

[19] J. Cui and X. Zhang, "Application of a multi-satellite dynamic mission scheduling model based on mission priority in emergency response," *Sensors*, vol. 19, no. 6, p. 1430, Mar. 2019, doi: 10.3390/s19061430.
[20] W. Yang, L. He, X. Liu, and Y. Chen, "Onboard coordination and scheduling of multiple autonomous satellites in an uncertain environment," *Adv. Space Res.*, vol. 68, no. 11, pp. 4505–4524, Dec. 2021, doi: 10.1016/j.asr.2021.09.003.
[21] J. Liang, Y.-H. Zhu, Y.-Z. Luo, J.-C. Zhang, and H. Zhu, "A precedence-rule-based heuristic for satellite onboard activity planning," *Acta Astronautica*, vol. 178, pp. 757–772, Jan. 2021, doi: 10.1016/j.actaastro.2020.10.020.
[22] W. Jianjiang, H. Xuejun, and H. Chuan, "Reactive scheduling of multiple EOSs under cloud uncertainties: Model and algorithms," *J. Syst. Eng. Electron.*, vol. 32, no. 1, pp. 163–177, Feb. 2021, doi: 10.23919/JSEE.2021.000015.
[23] C. Han, Y. Gu, G. Wu, and X. Wang, "Simulated annealing-based heuristic for multiple agile satellites scheduling under cloud coverage uncertainty," *IEEE Trans. Syst., Man, Cybern., Syst.*, vol. 53, no. 5, pp. 2863–2874, May 2023, doi: 10.1109/TSMC.2022.3220534.
[24] L. He, X.-L. Liu, Y.-W. Chen, L.-N. Xing, and K. Liu, "Hierarchical scheduling for real-time agile satellite task scheduling in a dynamic environment," *Adv. Space Res.*, vol. 63, no. 2, pp. 897–912, Jan. 2019, doi: 10.1016/j.asr.2018.10.007.
[25] Z. Lu, X. Shen, D. Li, D. Li, Y. Chen, D. Wang, and S. Shen, "Multiple super-agile satellite collaborative mission planning for area target imaging," *Int. J. Appl. Earth Observ. Geoinf.*, vol. 117, Mar. 2023, Art. no. 103211, doi: 10.1016/j.jag.2023.103211.
[26] Y. Xiao, S. Zhang, P. Yang, M. You, and J. Huang, "A two-stage flow-shop scheme for the multi-satellite observation and data-downlink scheduling problem considering weather uncertainties," *Rel. Eng. Syst. Saf.*, vol. 188, pp. 263–275, Aug. 2019, doi: 10.1016/j.ress.2019.03.016.
[27] Z. Zheng, J. Guo, and E. Gill, "Onboard autonomous mission re-planning for multi-satellite system," *Acta Astronautica*, vol. 145, pp. 28–43, Apr. 2018, doi: 10.1016/j.actaastro.2018.01.017.
[28] Y. Du, L. Xing, J. Zhang, Y. Chen, and Y. He, "MOEA based memetic algorithms for multi-objective satellite range scheduling problem," *Swarm Evol. Comput.*, vol. 50, Nov. 2019, Art. no. 100576, doi: 10.1016/j.swevo.2019.100576.
[29] X. Wang, G. Wu, L. Xing, and W. Pedrycz, "Agile earth observation satellite scheduling over 20 years: Formulations, methods, and future directions," *IEEE Syst. J.*, vol. 15, no. 3, pp. 3881–3892, Sep. 2021, doi: 10.1109/JSYST.2020.2997050.
[30] G. Chen, Y. Li, K. Zhang, X. Xue, J. Wang, Q. Luo, C. Yao, and J. Yao, "Efficient hierarchical surrogate-assisted differential evolution for high-dimensional expensive optimization," *Inf. Sci.*, vol. 542, pp. 228–246, Jan. 2021, doi: 10.1016/j.ins.2020.06.045.
[31] K. Cui, J. Song, L. Zhang, Y. Tao, W. Liu, and D. Shi, "Event-triggered deep reinforcement learning for dynamic task scheduling in multisatellite resource allocation," *IEEE Trans. Aerosp. Electron. Syst.*, vol. 59, no. 4, pp. 3766–3777, Aug. 2023, doi: 10.1109/TAES.2022.3231239.
[32] M. Wang and Y. Ma, "A differential evolution algorithm based on accompanying population and piecewise evolution strategy," *Appl. Soft Comput.*, vol. 143, Aug. 2023, Art. no. 110390, doi: 10.1016/j.asoc.2023.110390.
[33] Y. Wang, Z. Liu, and G.-G. Wang, "Improved differential evolution using two-stage mutation strategy for multimodal multi-objective optimization," *Swarm Evol. Comput.*, vol. 78, Apr. 2023, Art. no. 101232, doi: 10.1016/j.swevo.2023.101232.
[34] G. Li, W. Wang, C. Yue, W. Zhang, and Y. Wang, "Two-stage adaptive differential evolution with dynamic dual-populations for multimodal multi-objective optimization with local Pareto solutions," *Inf. Sci.*, vol. 644, Oct. 2023, Art. no. 119271, doi: 10.1016/j.ins.2023.119271.

XUEYING YANG was born in 1998. She received the B.S. degrees from Nanchang Hangkong University, Nanchang, China, in 2016 and 2020, respectively, and the M.S. degrees from the Belarusian State University of Informatics and Radioelectronics, Belarus, in 2020 and 2022, respectively. She is currently pursuing the Ph.D. degree in aeronautical and astronautical science and technology with Space Engineering University, Beijing, China. Her research interest includes multi-satellite mission planning and scheduling.

MIN HU was born in 1983. He received the B.S. and M.S. degrees from the Equipment College, China, in 2006 and 2008, respectively, and the Ph.D. degree from Space Engineering University, Beijing, China, in 2012. He is currently an Associate Professor with Space Engineering University. He has published more than 60 articles and authorized 25 national invention patents. His research interests include spacecraft orbit dynamics, distributed spacecraft dynamics and control, design of constellation, and space mission analysis.

GANG HUANG was born in Jiangsu, China, in 1991. He received the bachelor's degree from the Jincheng College, Nanjing University of Aeronautics and Astronautics, in 2015, and the master's degree from Nanchang Hangkong University, in 2020. He is currently pursuing the Ph.D. degree with Space Engineering University. His main research interests include evolutionary computing and intelligent collaboration.

ANDI LI was born in 2001. He received the B.S. degrees from Space Engineering University, Beijing, China, in 2019 and 2023, respectively, where he is currently pursuing the M.S. degree. His research interests include multi-satellite task planning and requirement processing.